Title

The *Arabidopsis* SR45 splicing factor bridges the splicing machinery and the exon-exon junction complex

Authors

Steven Fanara[1], Marie Schloesser[1], Marine Joris[1], Marylène Vandevenne[2], Marc Hanikenne[3†] and Patrick Motte[1†]

[1]InBioS-PhytoSystems, Functional Genomics and Plant Molecular Imaging, University of Liège, 4000, Liège, Belgium

[2]InBioS-Center for Protein Engineering, Laboratory of Biological Macromolecules, University of Liège, 4000, Liège, Belgium

[3]InBioS-PhytoSystems, Translational Plant Biology, University of Liège, 4000, Liège, Belgium

[†]These two authors contributed equally.

Email address for each author

Steven Fanara: steven.fanara@uliege.be

Marie Schloesser: mschloesser@uliege.be

Marine Joris: mjoris@uliege.be

Marylène Vandevenne: mvandevenne@uliege.be

Marc Hanikenne: marc.hanikenne@uliege.be

Patrick Motte: patrick.motte@uliege.be

Corresponding authors

Steven Fanara (steven.fanara@uliege.be; Tel: +32-4-366-38-11)

Correspondence may also be addressed to Patrick Motte (patrick.motte@uliege.be; Tel: +32-4-366-38-10)

University of Liège, InBioS-PhytoSystems

Quartier de la Vallée, 1

Chemin de la Vallée, 4 - Bât B22, B4000, Liège, Belgium

32 **Date of submission:** 07/08/2023

33

34 **Number of figures:** 8

35

36 **Word count:** 5340

37

38 **Number of supplementary figures:** 7

39

40 **Number of supplementary tables:** 15

41

42 **Running title**

43 Functional characterization of the SR45 splicing factor

44

Highlight

The nuclear localization of the Arabidopsis SR45 splicing factor and its ability to contact novel protein partners *in planta* and to specifically bind RNA motifs is controlled by critical residues.

Abstract

The Arabidopsis splicing factor serine/arginine-rich 45 (SR45) contributes to several biological processes. The *sr45-1* loss-of-function mutant exhibits delayed root development, late flowering, unusual numbers of floral organs, shorter siliques with decreased seed sets, narrower leaves and petals, and altered metal distribution. Here, we studied the function of each of SR45 domains by examining their involvement in: (i) the spatial distribution of SR45, (ii) the establishment of a protein-protein interaction network including spliceosomal and exon-exon junction complex (EJC) components, and (iii) the RNA binding specificity. We report that the endogenous *SR45* promoter is active during vegetative and reproductive growth, and that the SR45 protein localizes in the nucleus. We demonstrate that the C-terminal arginine/serine-rich domain is a determinant of nuclear localization. We show that the SR45 RNA recognition motif (RRM) domain specifically binds purine-rich RNA motifs via three residues (H101, H141, Y143), and is also involved in protein-protein interactions. We further show that SR45 bridges both mRNA splicing and surveillance machineries as a partner of EJC core components and peripheral factors, which requires phosphoresidues likely phosphorylated by kinases from both CLK and SRPK families. Our findings provide insights into the contribution of each SR45 domain to both spliceosome and EJC assemblies.

Keywords: Serine/arginine-rich splicing factor, SR45, Arabidopsis, splicing, exon-exon junction complex, EJC, protein-RNA and protein-protein interaction, ASAP, PSAP

Introduction

The precise recognition of splice sites at exon-intron boundaries is crucial in order to accurately perform pre-messenger RNA (pre-mRNA) splicing (Wahl *et al.*, 2009). While constitutive splicing results from the exclusion of each intron from the pre-mRNA, alternative splicing (AS) can lead to intron retention, shortened or lengthened exon or the skipping of an entire exon (Reddy *et al.*, 2013; Wang *et al.*, 2015). This occurs when weak or non-canonical splice sites are recognized and processed by the splicing machinery (Chen and Manley, 2009). It has important consequences for mRNA abundance and protein stability (Graveley, 2001). AS can be linked to an mRNA degrading process called NMD (AS-NMD) through the emergence of premature termination codons (PTCs) in alternatively spliced transcripts, which ultimately regulates transcript levels (Palusa and Reddy, 2010; Kalyna *et al.*, 2012). Protein isoforms that arise from alternative splicing usually differ in their primary sequence and domain organization which often alters their localization, stability, function or ability to interact with their protein or RNA partners (Laloum *et al.*, 2018).

Serine/arginine-rich (SR) proteins constitute a highly conserved family in multicellular eukaryotes (Califice *et al.*, 2012), sharing a modular structure characterized by the presence of one or two RNA recognition motif(s) [RRM(s)] in the N-terminus and a C-terminal domain rich in arginine-serine dipeptide repeats (RS) (Manley and Krainer, 2010; Califice *et al.*, 2012). While the RNA binding affinity is mainly dictated by the RRM domain (Maris *et al.*, 2005; Daubner *et al.*, 2013), the RS domain is involved in protein-RNA and protein-protein interactions through reversible phosphorylation (Xiao and Manley, 1997; Shen *et al.*, 2004; Schütze *et al.*, 2016; Schwich *et al.*, 2021). The phosphorylation status of the RS domain is controlled by at least two conserved protein kinase families, serine arginine protein kinases (SRPK) and *cdc2*-like kinases (CLK), as wells as some phosphatases (e.g., Protein Phosphatase 1, PP1) (Aubol *et al.*, 2016; Stankovic *et al.*, 2016; Aubol *et al.*, 2017). The SRPK kinases are located in the cytoplasm and the nucleus and strictly phosphorylate serine-arginine dipeptides (Ma *et al.*, 2009; Koutroumani *et al.*, 2017). They influence the localization of SR proteins by supporting their phosphorylation-dependant transport into the nucleus via an SR-specific transportin protein (TRN-SR, TNPO3) (Kataoka *et al.*, 1999; Lai *et al.*, 2000b; Lai *et al.*, 2001; Xu *et al.*, 2011). The CLK members are dual kinases and strictly nuclear (Lee *et al.*, 1996). They (auto-)phosphorylate not only serine-arginine but also serine-proline dipeptides (Lee *et al.*, 1996; Aubol *et al.*, 2013). Some SR

102 proteins display a nucleocytoplasmic dynamics and are known to play many additional roles in
103 (pre-)mRNA processing in mammals, including transcription, mRNA export (Huang and Steitz,
104 2001), stability and surveillance (Zhang and Krainer, 2004), and translation (Sanford *et al.*,
105 2004). The *Arabidopsis thaliana* (Arabidopsis) genome possesses nineteen SR protein-encoding
106 genes divided into seven subgroups, four of which are plant-specific because of a unique
107 multidomain structure (RS, SCL, RS2Z and SR45 subfamilies) (Barta *et al.*, 2010; Califice *et al.*,
108 2012).

109 SR45 is an atypical SR protein because it possesses a unique RRM flanked by one RS
110 domain on each side (Califice *et al.*, 2012), a domain organization similar to the one of the
111 human splicing factors Tra2β and RNPS1 (RNA-binding protein with Ser-rich domain 1) (Cléry
112 *et al.*, 2011), the human ortholog of SR45 (Califice *et al.*, 2012). RNPS1 plays critical roles in
113 splicing (Robinson *et al.*, 1999) and NMD by coupling the deposition of a quality control
114 complex (Exon Junction Complex, EJC) on spliced mRNAs to the UP-FRAMESHIFT (UPF)
115 protein complex, which consists of UPF1, UPF2 and UPF3 and triggers NMD (Lykke-Andersen
116 *et al.*, 2001). Two scaffold proteins, ACINUS and PININ, form with the EJC peripheral factors
117 RNPS1 and SAP18 the ternary complexes ASAP and PSAP, respectively, in order to regulate AS
118 and NMD (Sakashita *et al.*, 2004; Singh *et al.*, 2010; Murachelli *et al.*, 2012; Schlautmann *et al.*,
119 2022). The EJC itself is a conserved protein complex comprising four highly conserved core
120 proteins named eukaryotic initiation factor 4A3 (eIF4AIII), Mago nashi (MAGOH/Mago), Y14
121 and metastatic lymph node 51 (MLN51) (Tange *et al.*, 2005). The cytoplasmic disassembly of the
122 EJC results from the action of PYM (Bono et al., 2004). This EJC core serves as a platform for
123 multiple peripheral proteins in order to coordinate several steps of mRNA processing, namely
124 (alternative) splicing, intra-cellular RNA localization (which notably involves ALY/REF),
125 translation efficiency and mRNA stability control by NMD (Le Hir *et al.*, 2001; Nott *et al.*, 2004;
126 Singh *et al.*, 2012).

127 In Arabidopsis, little is known about the functional characteristics of the EJC components
128 and the associated peripheral factors (Chen *et al.*, 2019). The Arabidopsis homologues of MAGO,
129 Y14, PYM and eIF4AIII have been previously described (Johnson *et al.*, 2004; Park and Muench,
130 2007; Park *et al.*, 2009). MAGO and Y14 can heterodimerize (Park and Muench, 2007). While
131 the C-terminal portion of MAGO is critical for this interaction, it is dispensable for the
132 association with eIF4AIII (Cilano *et al.*, 2016). PYM interacts with the MAGO-Y14 complex, as

133 well as with the isolated proteins (Park and Muench, 2007). PYM and Y14 associate only when
134 both proteins are dephosphorylated, but the phosphorylation state does not affect the association
135 with MAGO (Mufarrege *et al.*, 2011). Knockdown of *MAGO* in plants leads to several
136 developmental defects, including vegetative and reproductive development impairment (Park *et*
137 *al.*, 2009). The DEAD-box RNA helicase eIF4AIII is a nuclear protein whose subcellular
138 localization is altered under hypoxia (Koroleva *et al.*, 2009). It interacts with ALY4 *in vitro* and
139 colocalizes with MAGO and Y14 *in planta* (Koroleva *et al.*, 2009). While RNPS1 was shown to
140 interact with Y14, no link was established between SR45 and Y14 or any other EJC core
141 component in Arabidopsis (Shi and Xu, 2003; Hsu Ia *et al.*, 2005; Wang *et al.*, 2018). However, it
142 was recently shown that ASAP and PSAP complexes containing SR45 exist in Arabidopsis and
143 contribute to the regulation of *FLC* expression (Qüesta *et al.*, 2016; Chen *et al.*, 2019; Bi *et al.*,
144 2021) and to the reproductive transition (Bi *et al.*, 2021). SR45 was shown to affect the
145 accumulation of ASAP protein components (Chen *et al.*, 2019).
146 As SR45 presents an atypical modular structure among SR proteins, with a unique RRM
147 flanked by one RS domain on both sides **(Supplementary Figure S1)**, the function of these
148 domains in the modulation of the SR45 splicing activity, i.e. its localization, ability to interact
149 with proteins and specificity of RNA binding, was examined. We first studied the expression
150 profile of *SR45* during plant development with native promoter-driven reporter constructs to link
151 previously described phenotypes of the loss-of-function mutant to the tissues where SR45 is
152 expressed. By substituting serines from both RS domains to alanines, we established that the
153 SR45 RS domains are required to retain the nuclear localization and play a key role in protein-
154 protein interactions. We further determined the RNA motif recognized by SR45 and demonstrated
155 how three amino acids in the RRM define the RNA binding specificity. Finally, we established
156 how phosphorylatable serines are critical for establishing the SR45 protein-protein interaction
157 network, particularly with kinases, EJC core components and EJC peripheral factors. Our
158 findings provide new insights into the involvement of SR45 in the recruitment of several splicing
159 factors and in EJC assembly.
160

161 **Materials and methods**

162 Plant material and growth conditions

163 Arabidopsis plants (Col-0 ecotype) were stably transformed by floral dipping, and
164 independent T3 homozygous lines were analyzed. All observations were performed in at least
165 three independent lines. Seeds were surface-sterilized, then germinated on 1/2 Murashige and
166 Skoog (MS) medium (Duchefa Biochimie) supplemented with sucrose (1% w/v, Duchefa
167 Biochimie) and Select Agar (0.8% w/v, Sigma-Aldrich) after stratification in the dark at 4°C for
168 48h. For expression profiling, 3-week-old seedlings were grown in hydroponic trays (Araponics)
169 in Hoagland medium for ten weeks (until silique development) as previously reported (Talke *et*
170 *al.*, 2006; Hanikenne *et al.*, 2008). Hydroponics were grown under a 16-h light (100 µmol m^{-2}
171 sec^{-1})/8-h dark regime in a climate-controlled growth chamber (21°C). The nutrient medium was
172 renewed with fresh solution once a week.

173 *Nicotiana tabacum* (cv Petit Havana) transient transformations by *Agrobacterium*
174 infiltration were performed as described (Rausin *et al.*, 2010; Stankovic *et al.*, 2016).

175

176 Vector constructions

177 All binary vector constructions and primers used in this study are listed and detailed in
178 **Supplementary Tables S1-9**. All PCRs were carried out using the Q5 DNA polymerase (NEB)
179 on Arabidopsis cDNA libraries or genomic DNA. All constructs were verified by sequencing. For
180 plant transient and stable transformations, all final plasmids were electroporated into the
181 *Agrobacterium tumefaciens* strain GV3101 (pMP90) and subsequently used for agroinfiltration or
182 floral dipping, respectively. All constructions contain the coding sequence of the *SR45.1* isoform,
183 which we name *SR45* hereafter (Zhang and Mount, 2009).

184 For yeast two- or three-hybrid assays (Y2H or Y3H), cDNAs coding for the potential
185 interactors were cloned into pGBKT7 and pGADT7 vectors (Clontech) using different restriction
186 sites, with the exception of the *SR45* and mutant variant coding sequences that were cloned into
187 pGBKT7(+) and pGADT7(+) in which *Asc*I and *Pac*I restriction sites were added (see
188 **Supplementary Tables S1 and S2** for primer lists).

189 The promoter region of *SR45* [1612 bp upstream of the ATG, as described by (Zhang and
190 Mount, 2009)] was amplified by PCR from genomic DNA. The promoter amplicon was ligated at
191 the *Sbf*I/*Kpn*I sites of the pMDC100 vector (Curtis and Grossniklaus, 2003) to create the

192 pMDC100:pSR45 vector. The *SR45* open reading frame (1242 bp, from the ATG to the last codon
193 before the stop codon) was then cloned at *Asc*I/*Pac*I sites to obtain pMDC100:pSR45:SR45 in
194 which a *nos* terminator (tNOS) was added between *Sac*I restriction sites. Finally, the EGFP
195 coding sequence was cloned at the *Pac*I site to create the pMDC100:pSR45:SR45:EGFP:tNOS
196 vector. To construct the pMDC32:pSR45:EGFP vector, the 2X35S promoter of the pMDC32
197 vector (Curtis and Grossniklaus, 2003) was replaced by the *SR45* promoter and EGFP was cloned
198 downstream of the promoter at *Kpn*I and *Sac*I restriction sites **(Supplementary Table S3)**.
199 The *SR45mutRRM* version was obtained by PCR-based site-directed mutagenesis as
200 described (Rausin *et al.*, 2010; Stankovic *et al.*, 2016) **(Supplementary Table S4)**. The other
201 mutated *SR45* versions were assembled by PCR from partially overlapping amplicons, which
202 corresponded to the coding sequence of each domain of SR45. They were amplified using either
203 the native *SR45* gene, the *SR45mutRRM* gene, or the two RS mutated domains (named RA1 and
204 RA2) synthesized by Eurofins Genomics (see **Supplementary Tables S5 and S6**). All assembled
205 mutant versions were then introduced into yeast vectors for Y2H (at *Asc*I/*Bam*HI) or pMDC32
206 fused to EGFP for protein localization (at *Asc*I/*Pac*I sites), respectively.
207 The BiFC constructs were obtained as described (Stankovic *et al.*, 2016) **(Supplementary**
208 **Table S7)**. The TriFC was performed with an additional plasmid, pMDC32 (Curtis and
209 Grossniklaus, 2003), containing no coding sequence or the one of either the RRM domain of
210 ACINUS (765 bp corresponding to the RRM domain, from the 1141st base to the stop codon and
211 preceded by an ATG codon) or PININ.
212 For SELEX experiments, genes encoding the RRM of SR45, and the RRM1 or the RRM2
213 of SR34 were cloned at *Bam*HI/*Eco*RI sites of the pGEX6P-1 as described (De Franco *et al.*,
214 2019) **(Supplementary Table S8)**. Sequences encoding mutated versions of RRM1 and RRM2
215 of SR34 were amplified from vectors previously described (Stankovic *et al.*, 2016).
216
217 <u>Yeast two- and three-hybrid systems</u>
218 The vectors and yeast (*Saccharomyces cerevisiae*) strains provided in the Matchmaker
219 Gold Yeast Two-Hybrid System (Clontech) were used to perform directed interaction analyses
220 (dY2H). Prior to (directed) Y2H experiments, toxicity and autoactivation of the wild-type *SR45*
221 and mutant variants were tested simultaneously on a medium -Trp/X-a-gal [for
222 pGBKT7/pGBKT7(+)] and -Leu/X-a-gal [for pGADT7/pGADT7(+)] using 100 ng of plasmid.

223 Yeast growth was not affected by any of the constructs, none of which led to autoactivation of the
224 reporter gene (*MEL1*) **(Supplementary Figure S2)**. Dimeric interactions were then tested on
225 selective medium -Trp/-Leu/-His/X-a-gal/Aureobasidin A.
226 For Y2H screening, the Y2HGold strain was transformed with the bait vector (pGBKT7-
227 SR45) and then mated with strain Y187 containing an Arabidopsis cDNA library (Mate and Plate
228 Library-Universal Arabidopsis, Clontech) (Stankovic *et al.*, 2016) or a custom cDNA library
229 made from entire mature leaf material (Make Your Own "Mate & Plate" Library System,
230 Clontech). Trimeric interactions (Y3H) were tested on selective medium -Met/-Trp/-Leu/-His /X-
231 a-gal/Aureobasidin A: yeast expressing SAP18 fused to the binding domain of GAL4 (using
232 SR45 as a bridge) were mated with yeast expressing either ACINUS or PININ fused to the
233 activation domain of GAL4.
234
235 Confocal Microscopy
236 Live cell imaging was performed on Leica TCS SP2 and SP5 inverted confocal laser
237 microscopes (Leica Microsystems). A water-immersion objective was used to collect images at
238 512x512 pixel resolution. EGFP was visualized using the 488-nm line of the argon laser, and the
239 emission light was dispersed and recorded at 500 to 560 nm (Rausin *et al.*, 2010; Stankovic *et al.*,
240 2016; Joris *et al.*, 2017). For BiFC and TriFC experiments, YFP was excited at 514 nm using the
241 argon laser and the emission light was recorded at 525 to 600 nm.
242
243 Analysis of the mRNA levels
244 100 mg of plant tissues were used to extract total RNA using NucleoSpin RNA Plant kit
245 (Macherey Nagel) as per manufacturer's instruction. cDNAs were synthesized from 1 µg of total
246 RNAs using the RevertAid H Minus First Strand cDNA Synthesis Kit (Fisher Scientific) with
247 oligo(dT) primers. Quantitative PCR reactions were performed in 384-well plates using a
248 QuantStudio5 system (Applied Biosystems) and Takyon Low Rox SYBR MasterMix dTTP Blue
249 (Eurogentec). Samples were obtained from three independent biological experiments. A total of
250 three technical replicates were performed for each combination of cDNA and primer pair
251 **(Supplementary Table S9)**. Gene expression was normalized relative to At1g58050 as described
252 (Pfaffl, 2001). *At1g58050* expression was the most stable gene among all tested references (*EF1α*
253 and *UBQ10*) (Czechowski *et al.*, 2005; Spielmann *et al.*, 2020).

254

255 Production of recombinant proteins

256 The recombinant protein production was performed using the expression vector pGEX6P-
257 1 in *E. coli* BL21(DE3) cells as described (De Franco *et al.*, 2019). Protein productions (native
258 and mutated RRM of SR45, or RRM1 or RRM2 of SR34) were carried out overnight at 18°C
259 upon induction with 0.5 mM IPTG. Lysis of the cells was carried out using a sonicator in 50 mM
260 Tris-HCl pH 8, 1 M NaCl, 2 mM $MgCl_2$, 1 mM dithiothreitol (DTT) and 1 mM PMSF. GST
261 fusion proteins were purified on Glutathione-Sepharose® 4B beads (GE Healthcare) and eluted
262 using a solution of 50 mM Tris-HCl pH 8, 100 mM NaCl, 1 mM dithiothreitol (DTT) and 35 mM
263 reduced glutathione.

264

265 SELEX experiments

266 The Systematic Evolution of Ligands by EXponential enrichment (SELEX) experiment
267 was performed using a randomized 25-nt DNA template library as previously reported (De
268 Franco *et al.*, 2019). 500 ng-1 µg of the purified template DNA library was used for the *in vitro*
269 transcription reaction (T7 RiboMAX™ Express Large Scale RNA Production System, Promega).
270 Unincorporated nucleotides were removed using mini Quick Spin RNA Columns (Roche). RNAs
271 were purified with phenol/chloroform and ethanol-precipitated. The RNA pellet was resuspended
272 in RNAse-free water, and the final RNA concentration was quantified by measuring the
273 absorbance at 260/280 nm. Binding reactions were carried out in 200 µL of SELEX buffer
274 (20 mM MOPS pH 7.0, 50 mM KCl, 5 mM $MgCl_2$, 1 mM DTT, 0.1% Triton-X-100, and 0.1 mM
275 PMSF) and included 80 pmol of GST-fused protein immobilized on GSH beads (GE Healthcare),
276 1–8 µg of heparin sulfate, and 0.8–4 nmol of RNAs. Samples were gently agitated at 4 °C for
277 60 min. Unbound RNA was removed by five consecutive bead washings in 500 µL of SELEX
278 buffer. HCl-25 mM glycine (pH 2.2) was used to dissociate RNA-protein complexes (25 °C,
279 5 min). Dissociated RNAs were purified using mini Quick Spin RNA Columns (Roche), then
280 ethanol-precipitated, and finally reverse-transcribed (SuperScript® III Reverse Transcriptase,
281 Invitrogen). The resulting cDNAs were PCR amplified by 10 cycles for SELEX rounds 1 to 3, or
282 15 cycles for last SELEX round. Amplification products were then purified (PCR clean up kit,
283 Thermo **Fisher Scientific)**. The amplified cDNAs were used as a template to synthesize a new
284 RNA library for the following SELEX rounds. In every SELEX round, selection stringency was

intensified by increasing the RNA/protein ratios and the heparin concentration. The final PCR products (round 4) were subcloned into the pJET vector (CloneJET PCR Cloning Kit, Thermo Fisher Scientific) and sequenced. The obtained sequences were analyzed using the MEME tool (version 5.4.1) (Bailey *et al.*, 2009), then logos were redesigned using the WebLogo software (Crooks *et al.*, 2004).

Statistical analysis

All data evaluation and statistics were performed using GraphPad Prism 7 (GraphPad Software v7.00). The replication level of each experiment is described in the Figure legends.

Accession numbers and information

All gene sequences are available through *The Arabidopsis Information Resource* (TAIR, http://www.arabidopsis.org/), with the accession numbers: Arabidopsis *SR45* (AT1G16610), *SC35* (AT5G64200), *SCL28* (AT5G18810), *SCL30* (AT3G55460), *SCL30a* (AT3G13570), *SCL33* (AT1G55310), *SR30* (AT1G09140), *SR34* (AT1G02840), *SR34a* (AT3G49430), *SR34b* (AT4G02430), *RS31* (AT3G61860), *RS31a* (AT2G46610), *RS40* (AT4G25500), *RS41* (AT5G52040), *RSZ21* (AT1G23860), *RSZ22* (AT4G31580), *RSZ22a* (AT2G24590), *RSZ232* (AT3G53500), *RS2Z33* (AT2G37340), *GRP7* (AT2G21660), *GRP8* (AT4G39260), *RZ-1B* (AT1G60650), *RZ-1C* (AT5G04280), *PRP38* (AT2G40650), *AFC1* (AT3G53570), *AFC2* (AT4G24740), *AFC3* (AT4G32660), *SRPK1* (AT4G35500), *SRPK2* (AT2G17530), *SRPK3a* (AT5G22840), *SRPK3b/SRPK5* (AT3G44850), *SRPK4* (AT3G53030), *Cyp59* (AT1G53720), *CypRS64* (AT3G63400), *Cyp65* (AT5G67530), *Cyp71* (AT3G44600), *CypRS92* (AT4G32420), *ACINUS* (AT4G39680), *ALY4* (AT5G37720), *eIF4A3* (AT3G19760), *MAGO* (AT1G02140), *PININ* (AT1G15200), *SAP18* (AT2G45640), *Y14* (AT1G51510), *MOS12* (AT2G26430), *MOS14* (AT5G62600).

310 **Results**

311 ***SR45 is expressed at all developmental stages***

312 During plant development, *SR45* was expressed to different extents in all vegetative and
313 floral organs examined as described by quantitative RT-PCR profiling **(Figure 1A)**. *SR45* was
314 significantly more expressed in inflorescences and young seedlings. The expression level was
315 lower and similar in whole roots, stems and (cauline) leaves. We also determined the spatial
316 expression pattern of *SR45* and the distribution of the protein using a GFP translational fusion
317 (*pSR45:SR45-EGFP*) **(Figure 1B-R)** and a promoter:reporter construct (*pSR45:EGFP*)
318 **(Supplementary Figure S3)**, respectively. Translational fusion lines confirmed (i) the spatial
319 transcriptional activity of the *SR45* promoter and (ii) the nuclear localization of SR45 (Ali *et al.*,
320 2003). The seed coat (including hilum) presented GFP fluorescence **(Figure 1B)**. Embryos
321 freshly dissected from seeds displayed fluorescence in cotyledons **(Figure 1C)**. Right after
322 germination, seedlings showed an intense fluorescence in all cell types within the radicle **(Figure**
323 **1D-E)**, the hypocotyl and the cotyledons **(Figure 1E)**. During vegetative growth, fluorescence
324 was detected in roots, root hairs **(Figure 1E-G)**, and leaves (including trichomes and stomata)
325 **(Figure 1I-J)** and was particularly visible within the vascular tissues of roots **(Figure 1F)**.
326 During flowering, the receptacle at the flower bases, together with the abscission zone and the
327 gynophore, emitted fluorescence signals **(Figure 1K)**. In flowers, GFP fluorescence resolved to
328 styles and stigmas, stamens (anthers and filaments but not pollen grains), petals (including veins),
329 and sepals **(Figure 1L-R)**. The observations in *pSR45:EGFP* lines were in agreement with those
330 of the *pSR45:SR45-EGFP* translational fusion lines. However, fluorescence of GFP alone, which
331 is not targeted to any specific subcellular compartment, was very weak, hence being sometimes
332 hardly detected above the background **(Supplementary Figure S3)**. Indeed, seeds, embryos and
333 radicles presented a low fluorescence signal in *pSR45:SR45-EGFP* lines that was fainter in
334 *pSR45:EGFP* lines.

335

336 ***Structural determinants modulating SR45 localization***

337 To understand the structural determinants modulating the SR45 cellular localization
338 **(Figure 1)**, we engineered seven mutant variants **(Supplementary Figure S1)**. First, the
339 canonical RRM of SR45, which is defined by a β_1-α_1-β_2-β_3-α_2-β_4 topology, was mutagenized at
340 conserved residues mediating RNA recognition in both RNP1 and RNP2 motifs (Cléry *et al.*,

341 2008). Both H101 (RNP2) and H141 (RNP1), together with Y143, were substituted to alanine to
342 create the SR45mutRRM variant. Second, all Ser residues were substituted to Ala within the RS1
343 (nt 1 to 291, 39 S-to-A substitutions) and/or RS2 (nt 529 to 1245, 49 S-to-A substitutions),
344 generating three variants (mutRS1, mutRS2, mutRS1+RS2), respectively. Finally, RRM and
345 RS1/RS2 mutations were combined, producing three more mutant variants (mutRS1+RRM,
346 mutRRM+RS2 and mutRS1+RRM+RS2).

347 After transient expression in tobacco leaf cells, no distinguishable changes appeared in the
348 protein localization of the SR45mutRS1 or SR45mutRRM variants **(Figure 2)** compared to the
349 native protein. In contrast, SR45mutRS2 partially accumulated in the cytoplasm in addition to a
350 nuclear localization. SR45mutRS1+RS2 showed nucleolar retention, whereas combining RS2
351 and RRM mutations (SR45mutRRM+RS2) noticeably increased the cytoplasmic retention
352 compared to the native protein and the SR45mutRS2 variant. With all substitutions combined
353 (SR45mutRS1+RRM+RS2), no fluorescence was detected within the nucleus, and only
354 cytoplasmic signal was observed. Altogether, the integrity of the RS2 domain appears necessary
355 but not sufficient for the nucleoplasmic localization of SR45.

356

357 ***SR45 interactome***

358 To identify interactors of SR45, two Arabidopsis cDNA libraries were screened using
359 yeast two-hybrid (Y2H). Four interactors were found: PRP38, RS2Z32, CypRS64, and MOS12.
360 These interactions were further confirmed by directed yeast two-hybrid assays (dY2H) **(Figure**
361 **3)**.

362 dY2H assays were performed to examine the SR45 interactions with kinases potentially
363 involved in RS domain phosphorylation, the 3 CLK kinases (AFC1-3) (Bender and Fink, 1994)
364 and the 5 SRPK kinases encoded in the Arabidopsis genome (Lorković *et al.*, 2004; de la Fuente
365 van Bentem *et al.*, 2006; Stankovic *et al.*, 2016). We confirmed that SR45 interacts with AFC2
366 (Golovkin and Reddy, 1999), and confirmed its recently reported interactions with SRPK3a,
367 SRPK3b [also named SRPK5 (Wang *et al.*, 2023)] and SRPK4. Among all SR45 mutant variants,
368 only RS1 mutations abolished the SRPK4- and AFC2-SR45 interactions, while RS1 or RS2
369 mutations both suppressed interactions with SRPK3a and SRPK3b/SRPK5 **(Figure 3)**. Those
370 results suggested that RS domains are involved in interactions with kinases.

371 SR45 interacts with several other SR proteins, namely SCL33, RSZ21, SR30, SR34,
372 SR34a, as well as other splicing factors such as the hnRNP-like proteins RZ-1B and RZ-1C
373 (Golovkin and Reddy, 1999; Zhang *et al.*, 2014; Stankovic *et al.*, 2016; Wu *et al.*, 2016). We
374 showed here that SR45 was able to interact with all SR proteins but itself (SR45.1 or SR45.2
375 splicing isoforms (Zhang and Mount, 2009)) **(Supplementary Figure S4)**. The integrity of both
376 RS domains was crucial for SR45 to contact SC35. In the cases of SR34, RS31a and SCL30, the
377 interactions were only weakened by mutations applied to either RS1 or RS2 but were completely
378 abolished for RS1/RS2 variants **(Figure 3)**. Instead, the RS1 variants showed suppressed
379 interactions with RS2Z32, RSZ21, RZ-1B, RZ-1C and MOS12. In contrast to interactions of
380 SR45 with SR proteins, the interactions with RZ-1B, RZ-1C or PRP38 were considerably
381 weakened upon substitutions in the RRM domain **(Figure 3)**. The SR45-PRP38 interaction was,
382 however, not affected by other substitutions **(Figure 3)**. SR45 contacted several nuclear
383 cyclophilins including Cyp59, CypRS64 and CypRS92, but not Cyp65 and Cyp71, which are all
384 involved in splicing regulation (Lorković *et al.*, 2004; Gullerova *et al.*, 2006; Barbosa Dos Santos
385 and Park, 2019). However, none of the mutant variants was able to maintain interactions with any
386 of the cyclophilins tested in yeast. No interaction was observed between SR45 and hnRNP-like
387 proteins GRP7 and GRP8 **(Figure 3)**.
388 In animals, several shuttling SR proteins (SRSF1, SRSF3 and SRSF7) act as adaptors for
389 mRNA nuclear export through the TAP/NXF1 machinery and compete with ALY/REF for
390 binding in the NXF1 complex (Huang *et al.*, 2003). A gene encoding a homolog of the human
391 TAP/NXF1 is missing in plant genomes (Merkle, 2011), but numerous ALY/REF orthologs were
392 discovered in Arabidopsis (Pfaff *et al.*, 2018; Ehrnsberger *et al.*, 2019). Our dY2H analysis
393 highlighted an interaction between SR45 and ALY4, which was tremendously weakened by RS1
394 and/or RRM mutations **(Figure 3)**. SR45 presents a nucleocytoplasmic dynamic whose nuclear
395 export is at least partly controlled by the XPO1-dependent export pathway (Stankovic *et al.*,
396 2016), whereas the nuclear import of plant SR proteins is likely driven by the activity of MOS14,
397 a transportin-SR (TRN-SR) (Xu *et al.*, 2011). Here, SR45 and MOS14 interacted, and the SR45
398 RS2 domain was required **(Figure 3)**.
399 The human RNPS1 contributes, together with SAP18, ACINUS and PININ, to the
400 edification of two EJC peripheral complexes, ASAP and PSAP (Sakashita *et al.*, 2004; Singh *et*
401 *al.*, 2010; Murachelli *et al.*, 2012). We next performed dY2H and directed yeast three-hybrid

402 (dY3H) assays to investigate interactions between SR45 with core (Y14, MAGO and eIF4AIII)
403 and peripheral (SAP18 and PININ, which are part of the ASAP and PSAP complexes,
404 respectively) components of the EJC **(Figure 3** and **Figure 4)**. We demonstrated that, unlike
405 eIF4AIII, MAGO and Y14 were able to interact with SR45, which required an intact RS1 domain
406 **(Figure 4A)**. We further confirmed that SR45 was able to interact with both ACINUS and PININ
407 (Qüesta *et al.*, 2016; Chen *et al.*, 2019; Bi *et al.*, 2021) but not SAP18 (Wang *et al.*, 2023).
408 SAP18 was not able to interact with either ACINUS or PININ **(Figure 4A)**, however, when the
409 three components were co-expressed in a Y3H system, an interaction was established between
410 SR45 and SAP18 through either ACINUS or PININ **(Figure 4B)**. The SR45-ACINUS interaction
411 was greatly diminished upon mutations in the RS1 domain **(Figure 4A)**. Based on animal models
412 where two conserved residues, a threonine and a tyrosine, are critical for the assembly of the
413 ASAP complex (Sakashita *et al.*, 2004; Singh *et al.*, 2010; Murachelli *et al.*, 2012), we identified
414 two amino acids (Thr607 and Tyr615) within the RRM domain of ACINUS that were expected to
415 be critical for the interaction with SR45. Accordingly, mutations of these two residues
416 (T607A/Y615A) abolished the interaction of ACINUS with SR45. On the other hand, the SR45-
417 PININ interaction was suppressed when mutations were present in the RRM of SR45 **(Figure**
418 **4A)**.
419 Altogether, our observations confirmed the importance of serine residues in the
420 establishment of interactions with kinases and splicing factors but also depicted a role for the
421 canonical RRM (through both RNP1 and RNP2 motifs) in the formation a protein complex
422 involved in mRNA export and mRNA surveillance.
423
424 ***The RS1 and RS2 domains of SR45 connect splicing factors and EJC peripheral factors in***
425 ***planta***
426 Observed in yeast, the interactions underlying the involvement of SR45 into the splicing
427 reaction (ACINUS, PININ and SR34) as well as the spliceosome catalytic activation (PRP38)
428 (Schütze *et al.*, 2016), which are also established by RNPS1 in human (Schütze *et al.*, 2016;
429 Schlautmann *et al.*, 2022), were further characterized in living plant cells using Yellow
430 Fluorescent Protein (YFP)-based bimolecular fluorescence complementation (BiFC). BiFC
431 experiments were performed in tobacco leaf cells where the native or mutant variants of SR45
432 fused to the C-terminal fragment of YFP (^{C}YFP) and interactors fused to the N-terminal fragment

433 of YFP (^{N}YFP) were transiently co-expressed. YFP fluorescence was observed in the nucleus and
434 in structures similar to nuclear speckles, suggesting that SR45 interactions with ACINUS, SR34
435 and PRP38 occurred in the nucleus and in splicing factors-enriched granules *in planta* **(Figure**
436 **5A)**. The study of mutant variants confirmed results obtained in yeast cells **(Figure 3)**, as
437 SR45mutRS1+RS2 was unable to interact with ACINUS and SR34, but remained able to
438 establish an interaction with PRP38 within the nucleolus. Trimolecular fluorescence
439 complementation (TriFC) also confirmed dY3H assays as SAP18 was unable to interact with
440 either SR45 or ACINUS **(Figure 5B, upper panels)** but was able to form trimeric ASAP and
441 PSAP complexes **(Figure 5B, lower panels)**.
442
443 ***Subcellular localization of SR45-associated partners***
444 To better decipher the dynamic phosphorylation of SR45 across cellular compartments
445 and where SR45 might precisely contact its (peripheral) EJC interactors in plant cells, EGFP was
446 fused to the N-terminus of candidate proteins, and translational fusions were transiently
447 expressed in tobacco leaf cells. SRPK1 and SRPK2, two non-interactors of SR45, resided
448 exclusively in the cytoplasm **(Figure 6)**. Unlike SRPK4 which resided predominantly in the
449 cytoplasm (alongside a weak detectable signal within the nucleus), SRPK3a and SRPK3b/SRPK5
450 localized in the cytoplasm and the nucleus **(Figure 6)**. The CLKs were the only kinases studied
451 that accumulated in nuclear speckles-like structures **(Figure 6)**. ACINUS, SAP18 and PININ all
452 localized in the nucleus, however, SAP18 also displayed a cytoplasmic localization **(Figure 6)**.
453 Similarly, MAGO and Y14 were also detected in the nucleus and in the cytoplasm **(Figure 6)**.
454 PRP38 localized in the nucleoplasm, speckles-like structures and the nucleolus **(Figure 6)**.
455 These observations suggest that the interactions described by dY2H/dY3H and
456 BiFC/TriFC may actually take place in plant cells, as the intracellular localization of SR45 and its
457 kinase and EJC interactors at least partially overlapped.
458
459 ***SR45 is binding to purine-rich RNA motifs***
460 Then, we investigated the RNA-binding specificity of a recombinant RRM domain of
461 SR45 fused to a glutathione-S-transferase using Systematic Evolution of Ligands by EXponential
462 enrichment (SELEX). Among the twelve clones sequenced after SELEX, two statistically
463 significant consensus sequences recognized by the SR45 RMM were identified, with a specificity

464 for a purine-rich central motif (5'-[A/G]GAAG-3') flanked by pyrimidine-rich regions (5'
465 UC[C/U] and 3' UU[C/U][C/U]C) (*E*-value: 8.6 x 10^{-4}) **(Figure 7A)** or for a purine-rich motif
466 ([A/G]GA[C/A]A) (*E*-value: 1.2 x 10^{-10}) **(Figure 7B)**. Because of the higher variability of bases
467 at most positions in the 2nd motif, we analyzed the 4-mer and 5-mer frequencies among the
468 sequences used to identify it. The analysis of 4-mer frequency showed a higher occurrence of the
469 GACA and GAAG motifs. The analysis of 5-mer frequency demonstrated higher prevalence of
470 AAGUU, AGACA, GAAGU, GACAU and AGAAG motifs **(Supplementary Table S10)**. This is
471 strikingly similar to G/A-rich motifs bound by RNPS1 (Mabin *et al.*, 2018).
472 To ensure the specificity of the binding of the identified RNA motifs to the SR45 RRM, a
473 mutated version (H101A, H141A and Y143A) was produced and studied in the SELEX set-up.
474 Four different sets of twelve sequences obtained using the mutated SR45 RRM were analyzed
475 **(Supplementary Table S11)** using the MEME tool. No enriched motif was discovered **(Figure**
476 **7C and Supplementary Figure S5)**, and the best motif recovered (lowest *E*-value, #4) did not
477 resemble significant motifs found for the native canonical RRM **(Figures 7A-B)**, indicating that
478 amino acids (H101, H141 and Y143) mutated within the RRM are necessary and sufficient to
479 ensure the accurate binding of SR45 to its purine-enriched target motif.
480

481 **Discussion**

482 Pre-mRNA splicing is a crucial step in the regulation of gene expression. Splice-site
483 selection is carried out by the binding of many *trans*-acting protein factors including the SR
484 splicing factors (Chen and Manley, 2009). In mammalian cells, it has been shown that SR
485 proteins regulate many aspects of gene expression (Huang and Steitz, 2001). In contrast, their
486 plant counterparts are mainly known to play important roles in constitutive splicing and
487 alternative splicing, in biological processes such as ABA signalling, salt response or metal
488 homeostasis (Xing *et al.*, 2015; Yan *et al.*, 2017; Zhang *et al.*, 2017; Fanara *et al.*, 2022) although
489 they are also suspected to be involved in other processes regulating gene expression, e.g. RNA-
490 directed DNA methylation and regulation of transcription (Rausin *et al.*, 2010; Ausin *et al.*, 2012;
491 Qüesta *et al.*, 2016; Stankovic *et al.*, 2016; Yan *et al.*, 2017; Bi *et al.*, 2021).

492

493 ***The RS domains of SR45 control its subcellular localization and protein-protein interaction***
494 ***network***

495 The SR45 splicing factor displays a modular structure, with two RS and one RRM
496 domains, which is atypical for a plant SR protein (Califice *et al.*, 2012). In this report, we
497 examined the involvement of each of these domains, as well as some of their constituent amino
498 acid residues, in molecular functions known to be regulated by the human ortholog of SR45
499 (RNPS1) (Califice *et al.*, 2012), whose association to EJC peripheral factors determines its roles
500 in pre-mRNA splicing, mRNA export and quality control (Le Hir *et al.*, 2016) **(Figure 8)**. We
501 show that a number of interactions between SR45 and spliceosomal or EJC components entirely
502 rely on the presence of serine residues in the RS domains of SR45. Indeed, the substitution of
503 only few residues in these domains can either tremendously diminish or abolish the connection
504 between SR45 and its partners, for instance the interactions with SR34 and other SR proteins.
505 Some of those serine residues also control the subcellular localization of SR45. S-to-A
506 substitutions within the RS2 domain alone induce cytoplasmic accumulation of SR45, which
507 might result from its inability to contact the plant transportin-SR (MOS14) that is thought to be
508 involved in the nuclear import of plant SR proteins (Xu *et al.*, 2011) as its human ortholog
509 TNPO3 (Maertens *et al.*, 2014; George *et al.*, 2019; Costa *et al.*, 2021). In contrast, S-to-A
510 substitutions in both RS domains strictly restrict SR45 to the nucleolus where it still can interact
511 with PRP38.

512 The nuclear import of SR proteins further depends on the phosphorylation of serine
513 residues present in the RS domain (Lai *et al.*, 2000a; Lai *et al.*, 2001). This process involves
514 several kinases in animals, mainly SRPK1 (ortholog of the Arabidopsis SRPK4) and CLK1
515 (ortholog of the Arabidopsis AFC2), which act together to regulate the phosphorylation status of
516 the human SRSF1 SR protein (Aubol *et al.*, 2016). We show here that in Arabidopsis, the
517 recognition of SR45 by two kinases of the SRPK family (SRPK3a and SRPK3b/SRPK5) depends
518 on the integrity of the RS2 domain. These kinases might therefore be predominately involved
519 (over other kinases) in the nuclear import of SR45 in conjunction with the transportin-SR
520 MOS14. While S-to-A substitutions within the RS2 does not affect the association between SR45
521 and SRPK4 or AFC2, all mutant variants harbouring RS1 substitutions were not able to contact
522 any of the kinases identified in this study. It is thus tempting to speculate that the RS1 domain of
523 SR45, which is essential for AFC2 and SRPK4 binding, might serve as a platform for
524 coordinating activity of these two kinases as seen in SRSF1 (Aubol *et al.*, 2017; Wegener and
525 Müller-McNicoll, 2019). A recent study identified specific serine residues within both RS
526 domains whose phosphorylation levels were downregulated in a *srpk3 srpk4 srpk3b/srpk5* triple
527 mutant, and tested interactions between these three kinases and SR45 mutant variants harbouring
528 phosphoresidue substitutions to alanine (Wang *et al.*, 2023). Here we focused on substituting all
529 serine within a domain to better decipher the importance of the global phosphorylation status to
530 (i) the subcellular localization of SR45 and (ii) to the protein-protein interaction network
531 established by this splicing factor. Both approaches uncovered similar results, as SRPK3, SRPK4
532 and SRPK3b/SRPK5 interactions with SR45 involve native serine residues within both RS
533 domains, i.e. S-to-A substitutions of all serines (this study) or of only phosphorylated serines
534 (Wang *et al.*, 2023) lead to the disruption of these interactions.
535
536 ***The SR45 RRM is essential to contact protein partners***
537 In the RRM of SR45, a histidine residue is present at the position of the putative aromatic
538 residue contacting RNA in both RNP2 (2nd position) and RNP1 (3rd position) motifs (Maris *et al.*,
539 2005; Cléry *et al.*, 2008; Daubner *et al.*, 2013) **(Supplementary Figure S1)**. Because histidine
540 residues are known to bind RNA molecules (Morozova *et al.*, 2006; Goroncy *et al.*, 2010), both
541 H101 (RNP2) and H141 (RNP1) together with Y143 were substituted by alanine to engineer the
542 SR45mutRRM variant. The data presented here suggest that the H101, H141 and Y143 residues

543 in the SR45 RRM are not structural determinants modulating SR45 localization. However, they
544 are critical to contact PININ and are partially involved in SR45 association to RZ-1B, RZ-1C,
545 ALY4 and PRP38. The suppression of contact between SR45 and PININ is in agreement with a
546 previous report establishing the involvement of the RRM of RNPS1 in the interaction with PININ
547 in mammals/humans (Murachelli *et al.*, 2012). Although RNPS1 edifies the ASAP complex with
548 ACINUS and SAP18 through its RRM (Murachelli *et al.*, 2012), SR45 contacts ACINUS using
549 preferentially the RS1 domain. This interaction is however completely abolished when S-to-A
550 substitutions are applied to both RS domains, which is in agreement with recent work (Wang *et*
551 *al.*, 2023). Based on the ASAP core structure previously published in animals (Murachelli *et al.*,
552 2012), we expected that ACINUS would contact SR45 through two residues (T607 and Y615)
553 located in the RRM. Accordingly, the substitutions T607A and Y615A abolished the interaction
554 between both partners in yeast. Our observations indicate that (i) the ASAP complex edifies in an
555 unexpected fashion (in comparison to animal models) that involves the RRM of ACINUS and at
556 least the RS1 domain of SR45, and (ii) the ASAP complex involves SAP18 as a ternary partner of
557 a pre-existing SR45-ACINUS platform as shown by Y3H and TriFC assays.
558
559 ***RNA binding specificity of the SR45 RRM***
560 So far, the characterization of RNA-binding specificity of plant SR proteins mainly in-
561 volved *in silico* analyses performed on RNA-Seq data generated from loss-of-function mutants.
562 Such an approach suggested that SCL30, one of the interactors of SR45, was able to bind to a
563 specific RNA sequence, 5'-AGAAGA-3' (Yan *et al.*, 2017). Four overrepresented RNA motifs
564 were also previously identified by the identification of direct RNA targets of SR45 (SR45-
565 associated RNAs, SARs) in seedlings (Xing *et al.*, 2015): the identified M1 and M4 motifs are
566 G/A-rich and were predicted to be predominately positioned within exons (Xing *et al.*, 2015); the
567 M2 and M3 motifs were U/C-rich and were preferentially located in intronic regions (Xing *et al.*,
568 2015). While the "Motif 1" identified here through SELEX cycles combined features of all the
569 motifs previously identified for SR45 (Xing *et al.*, 2015), the "Motif 2" contained invariant G/A
570 nucleotides and tend to be enriched in AGA, GGA and UCC trinucleotides **(Supplementary Fig-**
571 **ure S6)**. The human RNPS1 was found to be associated to G/A-rich 6-mers RNA regions (Mabin
572 *et al.*, 2018), which is reminiscent of the invariant sequence 5'-[A/G]GAAG-3' found here in
573 "Motif 1" associated to SR45. The RNA-binding specificity of the splicing factor and protein

partner of SR45, RZ-1C, was also determined by SELEX and involved G/A-rich motifs (Wu *et al.*, 2016). While the U/C-rich motif associated to SR45 is similar to the binding motifs of human NXF1 and SRSF3 in the 3'UTR of their target RNAs (Müller-McNicoll *et al.*, 2016), the ”Motif 1” is also strikingly similar to the binding motif of human NXF1 and of SRSF2, UPF3B and MLN51 (Hauer *et al.*, 2016; Wegener and Müller-McNicoll, 2019). Since plant genomes lack the *TAP/NXF1* gene (Serpeloni *et al.*, 2011), it is tempting to question the role of SR45 as an adaptor for the mRNA export machinery as previously reported for human SR proteins (Müller-McNicoll *et al.*, 2016). It is noteworthy that the SR45-associated ACINUS is known to bind both G/A-rich and U/C-rich motifs in humans (Rodor *et al.*, 2016). Different RNA motifs were uncovered for SR34 in this study **(Supplementary Figure S7 and Supplementary Tables S12-15)**, validating our SELEX approach capable of identify motifs specific to the studied RRM domain. Previous reports showed that purine-rich motifs, and specifically GAAG repeats, are typically related to positive splicing regulators (i.e. SR proteins) and are considered as exonic splicing enhancers (ESEs) in animals and plants (Fairbrother *et al.*, 2002; Pertea *et al.*, 2007; Thomas *et al.*, 2012; Wu *et al.*, 2014). Overall, this suggests that SR45 acts, to certain extent, as a positive regulator of alternative splicing (Xing *et al.*, 2015; Zhang *et al.*, 2017).

Competition between the dual roles of the SR45 RRM

Our results demonstrated that the RRM of SR45 is necessary to the edification of the PSAP complex and is able to efficiently bind RNA sequences. This dual role implies that its RNA binding ability would compete with the RRM contribution to protein complex edification, as previously described in the case of SRSF1 in animals (Aubol *et al.*, 2016; Wegener and Müller-McNicoll, 2019; Aubol *et al.*, 2021). The EJC components, Y14 and MAGO, mediate protein-protein interactions through the β-sheet surface of the RRM, which restricts the RNA binding ability of Y14 (Lau *et al.*, 2003; Shi and Xu, 2003). Although SR45 associates with EJC components and EJC peripheral factors, whether it is or not intrinsically involved in EJC-mediated molecular regulation and in underlying developmental processes still remains undetermined. It is worth noting that *acinus* and *pinin* loss-of-function mutants display phenotypes similar to a *sr45-1* mutant (i.e. dwarfism, delayed flowering, and ABA hypersensitivity) (Bi *et al.*, 2021).

605 ***Conclusion***

606 Here, we characterized the contribution of the RS and RRM, and their constitutive
607 residues, to the function of the Arabidopsis SR45 protein considering the many aspects defining a
608 splicing factor: (i) the subcellular localization, (ii) the ability to interact with protein partners, and
609 (iii) the specificity of the binding to RNA. Our results demonstrate a dual role for the RRM of
610 SR45 in both protein-protein and protein-RNA interactions, suggesting a possible competition
611 between both functions. Structural analysis will be useful to substantiate these findings, notably
612 in the presence of both a partner requiring the SR45 RRM to interact with and an RNA
613 specifically bound by this domain. Furthermore, it would be of interest to determine whether the
614 enrichment of the RNA motifs identified here also occurs within the pre-mRNA sequences of
615 direct RNA targets of SR45 and whether it is correlated to molecular changes in the expression
616 and in the splicing profiles of these targets. The latter would require the assessment of genome-
617 wide alternative splicing events occurring in the loss-of-function mutant *sr45-1* at developmental
618 stages displaying a higher abundance of SR45, such as in seedlings or in inflorescences as shown
619 here by our expression profiling. The mutant variants engineered in this study could serve in
620 complementation assays of the *sr45-1* mutant using native promoter-driven translational fusions.
621 This would demonstrate the importance of specific residues associated to a molecular function
622 (e.g. the specificity of RNA binding) for the physiological responses of the plant.

623

624 **<u>Supplementary data</u>**

625 **Supplementary Figure S1.** Scaled schemes depicting the native *SR45* gene and the engineered
626 mutant variants.

627 **Supplementary Figure S2.** Toxicity and autoactivation assays for yeast vectors harboring the
628 native *SR45* or mutant variant coding sequences.

629 **Supplementary Figure S3.** Reporter lines depicting the activity of the native *SR45* promoter
630 (*pSR45:EGFP*) at different developmental stages.

631 **Supplementary Figure S4.** SR45 interactions with all the nineteen Arabidopsis SR proteins.

632 **Supplementary Figure S5.** The mutated RRM of SR45 does not bind to any RNA consensus.

633 **Supplementary Figure S6.** Trinucleotide frequency among the sequences used to identify SR45-
634 associated RNA consensuses.

635 **Supplementary Figure S7.** RNA motifs binding to RRMs of SR34.

Supplementary Tables S1-9. List of primers used in this study, subdivided into experimental categories.

Supplementary Tables S10-15. List of sequences submitted to MEME to find significant consensus(es) for the native RRMs studied or to find non-significant motifs associated to mutated RRMs.

Acknowledgments

We thank Dr. Julien Spielmann, Dr. Simona De Franco and Prof. Moreno Galleni for helpful discussions.

Author contributions

PM conceived and directed the research. SF conducted most experiments, with contributions of MS, MJ and MV for SELEX experiments. PM and SF analyzed the data. PM and MH supervised experiments. SF made the figures. SF, MH and PM wrote the manuscript, with comments of MS.

Conflict of interest

No conflict of interest is declared.

Funding

Funding was provided by the "Fonds de la Recherche Scientifique–FNRS" (FRFC-1.E049.15, PDR-T.0206.13, CDR-J.0009.17, PDR-T0120.18, CDR-J.0082.21, PDR-T.0104.22). M.H. was Senior Research Associate of the F.R.S.-FNRS. S.F. was a doctoral fellow (F.R.I.A.). No conflict of interest declared.

Data availability

All data supporting the findings of the study are available within the paper and within its supplementary materials published online, or upon request.

References

Ali, G.S., Golovkin, M., and Reddy, A.S. (2003). Nuclear localization and *in vivo* dynamics of a plant-specific serine/arginine-rich protein. Plant J 36, 883-893.

Aubol, B.E., Hailey, K.L., Fattet, L., Jennings, P.A., and Adams, J.A. (2017). Redirecting SR Protein Nuclear Trafficking through an Allosteric Platform. J Mol Biol 429, 2178-2191.

Aubol, B.E., Plocinik, R.M., Hagopian, J.C., Ma, C.T., McGlone, M.L., Bandyopadhyay, R., Fu, X.D., and Adams, J.A. (2013). Partitioning RS domain phosphorylation in an SR protein through the CLK and SRPK protein kinases. J Mol Biol 425, 2894-2909.

Aubol, B.E., Wozniak, J.M., Fattet, L., Gonzalez, D.J., and Adams, J.A. (2021). CLK1 reorganizes the splicing factor U1-70K for early spliceosomal protein assembly. Proc Natl Acad Sci U S A 118.

Aubol, B.E., Wu, G., Keshwani, M.M., Movassat, M., Fattet, L., Hertel, K.J., Fu, X.D., and Adams, J.A. (2016). Release of SR Proteins from CLK1 by SRPK1: A Symbiotic Kinase System for Phosphorylation Control of Pre-mRNA Splicing. Mol Cell 63, 218-228.

Ausin, I., Greenberg, M.V., Li, C.F., and Jacobsen, S.E. (2012). The splicing factor SR45 affects the RNA-directed DNA methylation pathway in Arabidopsis. Epigenetics 7, 29-33.

Bailey, T.L., Boden, M., Buske, F.A., Frith, M., Grant, C.E., Clementi, L., Ren, J., Li, W.W., and Noble, W.S. (2009). MEME SUITE: tools for motif discovery and searching. Nucleic Acids Res 37, W202-208.

Barbosa Dos Santos, I., and Park, S.W. (2019). Versatility of Cyclophilins in Plant Growth and Survival: A Case Study in *Arabidopsis*. Biomolecules 9.

Barta, A., Kalyna, M., and Reddy, A.S. (2010). Implementing a rational and consistent nomenclature for serine/arginine-rich protein splicing factors (SR proteins) in plants. Plant Cell 22, 2926-2929.

Baxter, I., Hosmani, P.S., Rus, A., Lahner, B., Borevitz, J.O., Muthukumar, B., Mickelbart, M.V., Schreiber, L., Franke, R.B., and Salt, D.E. (2009). Root suberin forms an extracellular barrier that affects water relations and mineral nutrition in Arabidopsis. PLoS Genet 5, e1000492.

Bender, J., and Fink, G.R. (1994). AFC1, a LAMMER kinase from *Arabidopsis thaliana*, activates STE12-dependent processes in yeast. Proc Natl Acad Sci U S A 91, 12105-12109.

Bi, Y., Deng, Z., Ni, W., Shrestha, R., Savage, D., Hartwig, T., Patil, S., Hong, S.H., Zhang, Z., Oses-Prieto, J.A., Li, K.H., Quail, P.H., Burlingame, A.L., Xu, S.L., and Wang, Z.Y. (2021).

Arabidopsis ACINUS is O-glycosylated and regulates transcription and alternative splicing of regulators of reproductive transitions. Nat Commun 12, 945.

Califice, S., Baurain, D., Hanikenne, M., and Motte, P. (2012). A single ancient origin for prototypical serine/arginine-rich splicing factors. Plant Physiol 158, 546-560.

Chen, M., and Manley, J.L. (2009). Mechanisms of alternative splicing regulation: insights from molecular and genomics approaches. Nat Rev Mol Cell Biol 10, 741-754.

Chen, S.L., Rooney, T.J., Hu, A.R., Beard, H.S., Garrett, W.M., Mangalath, L.M., Powers, J.J., Cooper, B., and Zhang, X.N. (2019). Quantitative Proteomics Reveals a Role for SERINE/ARGININE-Rich 45 in Regulating RNA Metabolism and Modulating Transcriptional Suppression via the ASAP Complex in *Arabidopsis thaliana*. Front Plant Sci 10, 1116.

Cilano, K., Mazanek, Z., Khan, M., Metcalfe, S., and Zhang, X.N. (2016). A New Mutation, *hap1-2*, Reveals a C Terminal Domain Function in AtMago Protein and Its Biological Effects in Male Gametophyte Development in *Arabidopsis thaliana*. PLoS One 11, e0148200.

Cléry, A., Blatter, M., and Allain, F.H. (2008). RNA recognition motifs: boring? Not quite. Curr Opin Struct Biol 18, 290-298.

Cléry, A., Jayne, S., Benderska, N., Dominguez, C., Stamm, S., and Allain, F.H. (2011). Molecular basis of purine-rich RNA recognition by the human SR-like protein Tra2-β1. Nature structural & molecular biology 18, 443-450.

Costa, R., Rodia, M.T., Zini, N., Pegoraro, V., Marozzo, R., Capanni, C., Angelini, C., Lattanzi, G., Santi, S., and Cenacchi, G. (2021). Morphological study of TNPO3 and SRSF1 interaction during myogenesis by combining confocal, structured illumination and electron microscopy analysis. Mol Cell Biochem 476, 1797-1811.

Crooks, G.E., Hon, G., Chandonia, J.M., and Brenner, S.E. (2004). WebLogo: a sequence logo generator. Genome Res 14, 1188-1190.

Curtis, M.D., and Grossniklaus, U. (2003). A gateway cloning vector set for high-throughput functional analysis of genes in planta. Plant physiology 133, 462-469.

Czechowski, T., Stitt, M., Altmann, T., Udvardi, M.K., and Scheible, W.R. (2005). Genome-wide identification and testing of superior reference genes for transcript normalization in Arabidopsis. Plant Physiol 139, 5-17.

Daubner, G.M., Cléry, A., and Allain, F.H. (2013). RRM-RNA recognition: NMR or crystallography...and new findings. Curr Opin Struct Biol 23, 100-108.

De Franco, S., Vandenameele, J., Brans, A., Verlaine, O., Bendak, K., Damblon, C., Matagne, A., Segal, D.J., Galleni, M., Mackay, J.P., and Vandevenne, M. (2019). Exploring the suitability of RanBP2-type Zinc Fingers for RNA-binding protein design. Sci Rep 9, 2484.

de la Fuente van Bentem, S., Anrather, D., Roitinger, E., Djamei, A., Hufnagl, T., Barta, A., Csaszar, E., Dohnal, I., Lecourieux, D., and Hirt, H. (2006). Phosphoproteomics reveals extensive *in vivo* phosphorylation of Arabidopsis proteins involved in RNA metabolism. Nucleic Acids Res 34, 3267-3278.

Ehrnsberger, H.F., Grasser, M., and Grasser, K.D. (2019). Nucleocytosolic mRNA transport in plants : export factors and their influence on growth and development. J Exp Bot 70, 3757-3763.

Fairbrother, W.G., Yeh, R.F., Sharp, P.A., and Burge, C.B. (2002). Predictive identification of exonic splicing enhancers in human genes. Science 297, 1007-1013.

Fanara, S., Schloesser, M., Hanikenne, M., and Motte, P. (2022). Altered metal distribution in the *sr45-1* Arabidopsis mutant causes developmental defects. Plant J 110, 1332-1352.

George, A., Aubol, B.E., Fattet, L., and Adams, J.A. (2019). Disordered protein interactions for an ordered cellular transition: Cdc2-like kinase 1 is transported to the nucleus via its Ser-Arg protein substrate. J Biol Chem 294, 9631-9641.

Golovkin, M., and Reddy, A.S. (1999). An SC35-like protein and a novel serine/arginine-rich protein interact with *Arabidopsis* U1-70K protein. J Biol Chem 274, 36428-36438.

Goroncy, A.K., Koshiba, S., Tochio, N., Tomizawa, T., Inoue, M., Watanabe, S., Harada, T., Tanaka, A., Ohara, O., Kigawa, T., and Yokoyama, S. (2010). The NMR solution structures of the five constituent cold-shock domains (CSD) of the human UNR (upstream of N-ras) protein. J Struct Funct Genomics 11, 181-188.

Graveley, B.R. (2001). Alternative splicing: increasing diversity in the proteomic world. Trends Genet 17, 100-107.

Gullerova, M., Barta, A., and Lorković, Z.J. (2006). AtCyp59 is a multidomain cyclophilin from *Arabidopsis thaliana* that interacts with SR proteins and the C-terminal domain of the RNA polymerase II. RNA 12, 631-643.

Hanikenne, M., Talke, I.N., Haydon, M.J., Lanz, C., Nolte, A., Motte, P., Kroymann, J., Weigel, D., and Krämer, U. (2008). Evolution of metal hyperaccumulation required cis-regulatory changes and triplication of *HMA4*. Nature 453, 391-395.

Hauer, C., Sieber, J., Schwarzl, T., Hollerer, I., Curk, T., Alleaume, A.M., Hentze, M.W., and

Kulozik, A.E. (2016). Exon Junction Complexes Show a Distributional Bias toward Alternatively Spliced mRNAs and against mRNAs Coding for Ribosomal Proteins. Cell Rep 16, 1588-1603.

Hsu Ia, W., Hsu, M., Li, C., Chuang, T.W., Lin, R.I., and Tarn, W.Y. (2005). Phosphorylation of Y14 modulates its interaction with proteins involved in mRNA metabolism and influences its methylation. J Biol Chem 280, 34507-34512.

Huang, Y., Gattoni, R., Stévenin, J., and Steitz, J.A. (2003). SR splicing factors serve as adapter proteins for TAP-dependent mRNA export. Mol Cell 11, 837-843.

Huang, Y., and Steitz, J.A. (2001). Splicing factors SRp20 and 9G8 promote the nucleocytoplasmic export of mRNA. Mol Cell 7, 899-905.

Johnson, M.A., von Besser, K., Zhou, Q., Smith, E., Aux, G., Patton, D., Levin, J.Z., and Preuss, D. (2004). Arabidopsis *hapless* mutations define essential gametophytic functions. Genetics 168, 971-982.

Joris, M., Schloesser, M., Baurain, D., Hanikenne, M., Muller, M., and Motte, P. (2017). Number of inadvertent RNA targets for morpholino knockdown in *Danio rerio* is largely underestimated: evidence from the study of Ser/Arg-rich splicing factors. Nucleic Acids Res 45, 9547-9557.

Kalyna, M., Simpson, C.G., Syed, N.H., Lewandowska, D., Marquez, Y., Kusenda, B., Marshall, J., Fuller, J., Cardle, L., McNicol, J., Dinh, H.Q., Barta, A., and Brown, J.W. (2012). Alternative splicing and nonsense-mediated decay modulate expression of important regulatory genes in *Arabidopsis*. Nucleic Acids Res 40, 2454-2469.

Kataoka, N., Bachorik, J.L., and Dreyfuss, G. (1999). Transportin-SR, a nuclear import receptor for SR proteins. J Cell Biol 145, 1145-1152.

Koroleva, O.A., Calder, G., Pendle, A.F., Kim, S.H., Lewandowska, D., Simpson, C.G., Jones, I.M., Brown, J.W., and Shaw, P.J. (2009). Dynamic behavior of *Arabidopsis* eIF4A-III, putative core protein of exon junction complex: fast relocation to nucleolus and splicing speckles under hypoxia. Plant Cell 21, 1592-1606.

Koutroumani, M., Papadopoulos, G.E., Vlassi, M., Nikolakaki, E., and Giannakouros, T. (2017). Evidence for disulfide bonds in SR Protein Kinase 1 (SRPK1) that are required for activity and nuclear localization. PLoS One 12, e0171328.

Lai, M.C., Lin, R.I., Huang, S.Y., Tsai, C.W., and Tarn, W.Y. (2000a). A human importin-beta family protein, transportin-SR2, interacts with the phosphorylated RS domain of SR proteins. J Biol Chem 275, 7950-7957.

Lai, M.C., Lin, R.I., Huang, S.Y., Tsai, C.W., and Tarn, W.Y. (2000b). A human importin-*β* family protein, transportin-SR2, interacts with the phosphorylated RS domain of SR proteins. The Journal of biological chemistry 275, 7950-7957.

Lai, M.C., Lin, R.I., and Tarn, W.Y. (2001). Transportin-SR2 mediates nuclear import of phosphorylated SR proteins. Proc Natl Acad Sci U S A 98, 10154-10159.

Laloum, T., Martín, G., and Duque, P. (2018). Alternative Splicing Control of Abiotic Stress Responses. Trends Plant Sci 23, 140-150.

Lau, C.K., Diem, M.D., Dreyfuss, G., and Van Duyne, G.D. (2003). Structure of the Y14-Magoh core of the exon junction complex. Curr Biol 13, 933-941.

Le Hir, H., Gatfield, D., Izaurralde, E., and Moore, M.J. (2001). The exon-exon junction complex provides a binding platform for factors involved in mRNA export and nonsense-mediated mRNA decay. EMBO J 20, 4987-4997.

Le Hir, H., Saulière, J., and Wang, Z. (2016). The exon junction complex as a node of post-transcriptional networks. Nat Rev Mol Cell Biol 17, 41-54.

Lee, K., Du, C., Horn, M., and Rabinow, L. (1996). Activity and autophosphorylation of LAMMER protein kinases. J Biol Chem 271, 27299-27303.

Lorković, Z.J., Lopato, S., Pexa, M., Lehner, R., and Barta, A. (2004). Interactions of *Arabidopsis* RS domain containing cyclophilins with SR proteins and U1 and U11 small nuclear ribonucleoprotein-specific proteins suggest their involvement in pre-mRNA Splicing. J Biol Chem 279, 33890-33898.

Lykke-Andersen, J., Shu, M.D., and Steitz, J.A. (2001). Communication of the position of exon-exon junctions to the mRNA surveillance machinery by the protein RNPS1. Science 293, 1836-1839.

Ma, C.T., Hagopian, J.C., Ghosh, G., Fu, X.D., and Adams, J.A. (2009). Regiospecific phosphorylation control of the SR protein ASF/SF2 by SRPK1. J Mol Biol 390, 618-634.

Mabin, J.W., Woodward, L.A., Patton, R.D., Yi, Z., Jia, M., Wysocki, V.H., Bundschuh, R., and Singh, G. (2018). The Exon Junction Complex Undergoes a Compositional Switch that Alters mRNP Structure and Nonsense-Mediated mRNA Decay Activity. Cell Rep 25, 2431-2446 e2437.

Maertens, G.N., Cook, N.J., Wang, W., Hare, S., Gupta, S.S., Öztop, I., Lee, K., Pye, V.E., Cosnefroy, O., Snijders, A.P., KewalRamani, V.N., Fassati, A., Engelman, A., and Cherepanov, P. (2014). Structural basis for nuclear import of splicing factors by human Transportin 3. Proc Natl

Acad Sci U S A 111, 2728-2733.

Manley, J.L., and Krainer, A.R. (2010). A rational nomenclature for serine/arginine-rich protein splicing factors (SR proteins). Genes Dev 24, 1073-1074.

Maris, C., Dominguez, C., and Allain, F.H. (2005). The RNA recognition motif, a plastic RNA-binding platform to regulate post-transcriptional gene expression. FEBS J 272, 2118-2131.

Merkle, T. (2011). Nucleo-cytoplasmic transport of proteins and RNA in plants. Plant Cell Rep 30, 153-176.

Morozova, N., Allers, J., Myers, J., and Shamoo, Y. (2006). Protein-RNA interactions: exploring binding patterns with a three-dimensional superposition analysis of high resolution structures. Bioinformatics 22, 2746-2752.

Mufarrege, E.F., Gonzalez, D.H., and Curi, G.C. (2011). Functional interconnections of *Arabidopsis* exon junction complex proteins and genes at multiple steps of gene expression. J Exp Bot 62, 5025-5036.

Müller-McNicoll, M., Botti, V., de Jesus Domingues, A.M., Brandl, H., Schwich, O.D., Steiner, M.C., Curk, T., Poser, I., Zarnack, K., and Neugebauer, K.M. (2016). SR proteins are NXF1 adaptors that link alternative RNA processing to mRNA export. Genes Dev 30, 553-566.

Murachelli, A.G., Ebert, J., Basquin, C., Le Hir, H., and Conti, E. (2012). The structure of the ASAP core complex reveals the existence of a Pinin-containing PSAP complex. Nat Struct Mol Biol 19, 378-386.

Nott, A., Le Hir, H., and Moore, M.J. (2004). Splicing enhances translation in mammalian cells: an additional function of the exon junction complex. Genes Dev 18, 210-222.

Palusa, S.G., and Reddy, A.S. (2010). Extensive coupling of alternative splicing of pre-mRNAs of serine/arginine (SR) genes with nonsense-mediated decay. New Phytol 185, 83-89.

Park, N.I., and Muench, D.G. (2007). Biochemical and cellular characterization of the plant ortholog of PYM, a protein that interacts with the exon junction complex core proteins Mago and Y14. Planta 225, 625-639.

Park, N.I., Yeung, E.C., and Muench, D.G. (2009). Mago Nashi is involved in meristem organization, pollen formation, and seed development in Arabidopsis. Plant Sci 176, 461-469.

Pertea, M., Mount, S.M., and Salzberg, S.L. (2007). A computational survey of candidate exonic splicing enhancer motifs in the model plant *Arabidopsis thaliana*. BMC Bioinformatics 8, 159.

Pfaff, C., Ehrnsberger, H.F., Flores-Tornero, M., Sørensen, B.B., Schubert, T., Längst, G.,

Griesenbeck, J., Sprunck, S., Grasser, M., and Grasser, K.D. (2018). ALY RNA-Binding Proteins Are Required for Nucleocytosolic mRNA Transport and Modulate Plant Growth and Development. Plant Physiol 177, 226-240.

Pfaffl, M.W. (2001). A new mathematical model for relative quantification in real-time RT-PCR. Nucleic Acids Res 29, e45.

Qüesta, J.I., Song, J., Geraldo, N., An, H., and Dean, C. (2016). *Arabidopsis* transcriptional repressor VAL1 triggers Polycomb silencing at *FLC* during vernalization. Science 353, 485-488.

Rausin, G., Tillemans, V., Stankovic, N., Hanikenne, M., and Motte, P. (2010). Dynamic nucleocytoplasmic shuttling of an Arabidopsis SR splicing factor: role of the RNA-binding domains. Plant Physiol 153, 273-284.

Reddy, A.S., Marquez, Y., Kalyna, M., and Barta, A. (2013). Complexity of the alternative splicing landscape in plants. Plant Cell 25, 3657-3683.

Robinson, N.J., Procter, C.M., Connolly, E.L., and Guerinot, M.L. (1999). A ferric-chelate reductase for iron uptake from soils. Nature 397, 694-697.

Rodor, J., Pan, Q., Blencowe, B.J., Eyras, E., and Cáceres, J.F. (2016). The RNA-binding profile of Acinus, a peripheral component of the exon junction complex, reveals its role in splicing regulation. RNA 22, 1411-1426.

Sakashita, E., Tatsumi, S., Werner, D., Endo, H., and Mayeda, A. (2004). Human RNPS1 and its associated factors: a versatile alternative pre-mRNA splicing regulator in vivo. Mol Cell Biol 24, 1174-1187.

Sanford, J.R., Gray, N.K., Beckmann, K., and Cáceres, J.F. (2004). A novel role for shuttling SR proteins in mRNA translation. Genes Dev 18, 755-768.

Schlautmann, L.P., Lackmann, J.W., Altmüller, J., Dieterich, C., Boehm, V., and Gehring, N.H. (2022). Exon junction complex-associated multi-adapter RNPS1 nucleates splicing regulatory complexes to maintain transcriptome surveillance. Nucleic Acids Res 50, 5899-5918.

Schütze, T., Ulrich, A.K., Apelt, L., Will, C.L., Bartlick, N., Seeger, M., Weber, G., Lührmann, R., Stelzl, U., and Wahl, M.C. (2016). Multiple protein-protein interactions converging on the Prp38 protein during activation of the human spliceosome. RNA 22, 265-277.

Schwich, O.D., Blümel, N., Keller, M., Wegener, M., Setty, S.T., Brunstein, M.E., Poser, I., Mozos, I.R.L., Suess, B., Münch, C., McNicoll, F., Zarnack, K., and Müller-McNicoll, M. (2021). SRSF3 and SRSF7 modulate 3'UTR length through suppression or activation of proximal

polyadenylation sites and regulation of CFIm levels. Genome Biol 22, 82.

Serpeloni, M., Vidal, N.M., Goldenberg, S., Ávila, A.R., and Hoffmann, F.G. (2011). Comparative genomics of proteins involved in RNA nucleocytoplasmic export. BMC Evol Biol 11, 7.

Shen, H., Kan, J.L., and Green, M.R. (2004). Arginine-serine-rich domains bound at splicing enhancers contact the branchpoint to promote prespliceosome assembly. Mol Cell 13, 367-376.

Shi, H., and Xu, R.M. (2003). Crystal structure of the *Drosophila* Mago nashi-Y14 complex. Genes Dev 17, 971-976.

Singh, G., Kucukural, A., Cenik, C., Leszyk, J.D., Shaffer, S.A., Weng, Z., and Moore, M.J. (2012). The cellular EJC interactome reveals higher-order mRNP structure and an EJC-SR protein nexus. Cell 151, 750-764.

Singh, K.K., Erkelenz, S., Rattay, S., Dehof, A.K., Hildebrandt, A., Schulze-Osthoff, K., Schaal, H., and Schwerk, C. (2010). Human SAP18 mediates assembly of a splicing regulatory multiprotein complex via its ubiquitin-like fold. RNA 16, 2442-2454.

Spielmann, J., Ahmadi, H., Scheepers, M., Weber, M., Nitsche, S., Carnol, M., Bosman, B., Kroymann, J., Motte, P., Clemens, S., and Hanikenne, M. (2020). The two copies of the zinc and cadmium ZIP6 transporter of *Arabidopsis halleri* have distinct effects on cadmium tolerance. Plant Cell Environ 43, 2143-2157.

Stankovic, N., Schloesser, M., Joris, M., Sauvage, E., Hanikenne, M., and Motte, P. (2016). Dynamic Distribution and Interaction of the Arabidopsis SRSF1 Subfamily Splicing Factors. Plant Physiol 170, 1000-1013.

Talke, I.N., Hanikenne, M., and Krämer, U. (2006). Zinc-dependent global transcriptional control, transcriptional deregulation, and higher gene copy number for genes in metal homeostasis of the hyperaccumulator *Arabidopsis halleri*. Plant Physiol 142, 148-167.

Tange, T.O., Shibuya, T., Jurica, M.S., and Moore, M.J. (2005). Biochemical analysis of the EJC reveals two new factors and a stable tetrameric protein core. RNA 11, 1869-1883.

Thomas, J., Palusa, S.G., Prasad, K.V., Ali, G.S., Surabhi, G.K., Ben-Hur, A., Abdel-Ghany, S.E., and Reddy, A.S. (2012). Identification of an intronic splicing regulatory element involved in auto-regulation of alternative splicing of *SCL33* pre-mRNA. Plant J 72, 935-946.

Wahl, M.C., Will, C.L., and Lührmann, R. (2009). The spliceosome: design principles of a dynamic RNP machine. Cell 136, 701-718.

Wang, T., Wang, X., Wang, H., Yu, C., Xiao, C., Zhao, Y., Han, H., Zhao, S., Shao, Q., Zhu, J., Zhao, Y., Wang, P., and Ma, C. (2023). *Arabidopsis* SRPKII family proteins regulate flowering via phosphorylation of SR proteins and effects on gene expression and alternative splicing. New Phytol 238, 1889-1907.

Wang, Y., Liu, J., Huang, B.O., Xu, Y.M., Li, J., Huang, L.F., Lin, J., Zhang, J., Min, Q.H., Yang, W.M., and Wang, X.Z. (2015). Mechanism of alternative splicing and its regulation. Biomed Rep 3, 152-158.

Wang, Z., Ballut, L., Barbosa, I., and Le Hir, H. (2018). Exon Junction Complexes can have distinct functional flavours to regulate specific splicing events. Sci Rep 8, 9509.

Weber, M., Harada, E., Vess, C., Roepenack-Lahaye, E., and Clemens, S. (2004). Comparative microarray analysis of *Arabidopsis thaliana* and *Arabidopsis halleri* roots identifies nicotianamine synthase, a ZIP transporter and other genes as potential metal hyperaccumulation factors. Plant J 37, 269-281.

Wegener, M., and Müller-McNicoll, M. (2019). View from an mRNP: The Roles of SR Proteins in Assembly, Maturation and Turnover. Adv Exp Med Biol 1203, 83-112.

Wu, H.P., Su, Y.S., Chen, H.C., Chen, Y.R., Wu, C.C., Lin, W.D., and Tu, S.L. (2014). Genome-wide analysis of light-regulated alternative splicing mediated by photoreceptors in *Physcomitrella patens*. Genome Biol 15, R10.

Wu, Z., Zhu, D., Lin, X., Miao, J., Gu, L., Deng, X., Yang, Q., Sun, K., Zhu, D., Cao, X., Tsuge, T., Dean, C., Aoyama, T., Gu, H., and Qu, L.J. (2016). RNA Binding Proteins RZ-1B and RZ-1C Play Critical Roles in Regulating Pre-mRNA Splicing and Gene Expression during Development in Arabidopsis. Plant Cell 28, 55-73.

Xiao, S.H., and Manley, J.L. (1997). Phosphorylation of the ASF/SF2 RS domain affects both protein-protein and protein-RNA interactions and is necessary for splicing. Genes Dev 11, 334-344.

Xing, D., Wang, Y., Hamilton, M., Ben-Hur, A., and Reddy, A.S. (2015). Transcriptome-Wide Identification of RNA Targets of Arabidopsis SERINE/ARGININE-RICH45 Uncovers the Unexpected Roles of This RNA Binding Protein in RNA Processing. Plant Cell 27, 3294-3308.

Xu, S., Zhang, Z., Jing, B., Gannon, P., Ding, J., Xu, F., Li, X., and Zhang, Y. (2011). Transportin-SR is required for proper splicing of *Resistance* genes and plant immunity. PLoS Genet 7, e1002159.

Yan, Q., Xia, X., Sun, Z., and Fang, Y. (2017). Depletion of *Arabidopsis* SC35 and SC35-like serine/arginine-rich proteins affects the transcription and splicing of a subset of genes. PLoS Genet 13, e1006663.

Zhang, X.N., Mo, C., Garrett, W.M., and Cooper, B. (2014). Phosphothreonine 218 is required for the function of SR45.1 in regulating flower petal development in *Arabidopsis*. Plant Signal Behav 9, e29134.

Zhang, X.N., and Mount, S.M. (2009). Two alternatively spliced isoforms of the Arabidopsis SR45 protein have distinct roles during normal plant development. Plant Physiol 150, 1450-1458.

Zhang, X.N., Shi, Y., Powers, J.J., Gowda, N.B., Zhang, C., Ibrahim, H.M.M., Ball, H.B., Chen, S.L., Lu, H., and Mount, S.M. (2017). Transcriptome analyses reveal SR45 to be a neutral splicing regulator and a suppressor of innate immunity in *Arabidopsis thaliana*. BMC Genomics 18, 772.

Zhang, Z., and Krainer, A.R. (2004). Involvement of SR proteins in mRNA surveillance. Mol Cell 16, 597-607.

Figure legends

Figure 1. Expression profile of the *SR45* gene and of the corresponding protein. **(A)** Quantitative RT-PCR analyses of *SR45* gene expression in Arabidopsis vegetative and reproductive organs. Values represent means ± SEM (from three biological replicates, each consisting of pools of organs from three plants) and are relative to *AT1G58050*. Data were analyzed by one-way ANOVA followed by Dunnett multiple comparison post-tests. Statistically significant differences between means are indicated different letters ($P<0.05$). (**B-R**) Expression profile of the SR45 protein. The fusion protein SR45:GFP is expressed in **(B)** seed coat and hilum region, **(C)** embryo (cotyledons), **(D)** radicle, **(E)** young seedling (cotyledons and root, including root hairs as indicated by the arrow), **(F-H)** two-week-old root vasculature **(F, H)** and epidermis **(G)**, **(I-J)** leaves, including stomata [**(I)**, arrow] and trichome [**(J)**, arrow], **(K-L)** gynoecium (valves, gynophore, abscission zone and receptacle) **(K)**, and stigma and style **(L)**, **(M-N)** androecium (anther and filament), **(O-Q)** petals (epidermis and veins), and **(R)** sepal epidermis. Red signals represent chlorophyll autofluoresence. At least three independent T3 lines were generated and analyzed, depicting similar fluorescence profiles.

Figure 2. Structural determinants modulating SR45 localization. Subcellular fluorescence distribution in transient expression assays in tobacco leaf cells upon N-terminal EGFP-tagging of the native SR45 and SR45 mutant variants. Dotted lines delimit the nucleus. Scale bars = 10 µm. Red signals represent chlorophyll autofluoresence. Whenever cytoplasmic and nuclear signals were detected, insets depict the detailed intranuclear localization. At least three independent transient events were generated and analyzed, depicting similar fluorescence profiles.

Figure 3. SR45 interactions detected by (directed) yeast two-hybrid screenings. From the mated culture, dilutions to an OD600 of 1 were spotted on -Trp/-Leu/-His/X-α-Gal/AurA agar plates. Positive interactions were confirmed by growth and blue staining as seen with the positive control (pGADT7-T x pGBKT7-53). Purple and red squares are indicative of a weakened or abolished interaction upon substitutions within the corresponding SR45 domain, respectively. A weakened interaction is characterized by the ability of several single colonies to grow, while an abolished interaction is characterized at most by a white halo of dead cells (similar to the negative control pGADT7-T x pGBKT7-Lam).

Figure 4. SR45 associates with EJC core components and peripheral factors. Interaction between the native SR45, and SR45 mutant variants, and ACINUS(RRM) and PININ (from plant ASAP and PSAP complexes, respectively), and EJC core components (MAGO and Y14) **(A)**. Ternary complexes formed in the simultaneous presence of SAP18, SR45 and either ACINUS(RRM) or PININ **(B)**. From the mated culture, dilutions to an OD600 of 1 were spotted on -Trp/-Leu/-His/X-α-Gal/AurA agar plates (for Y2H assays) **(A)** or -Met/-Trp/-Leu/-His /X-a-gal/Aureobasidin A (for Y3H assays) **(B)**. Positive interactions were confirmed by growth and blue staining. Purple and red squares are indicative of a weakened or abolished interaction upon substitutions within the corresponding SR45 domain, respectively. A weakened interaction is characterized by the ability of several single colonies to grow, while an abolished interaction is characterized at most by a white halo of dead cells.

Figure 5. SR45 interacts with splicing factors and EJC peripheral factors in plant cells. **(A)** Bimolecular Fluorescence Complementation (BiFC) through co-expression of SR45 or SR45 mutant variants fused to the C-terminal half of YFP (SR45, SR45mutRS1, or SR45mutRS1+RS2:^{C}YFP) and ACINUS(RRM), SR34, or PRP38 fused to the N-terminal half of YFP (ACINUS(RRM), SR34, or PRP38:^{N}YFP). Dotted lines delimit the nucleus. **(B)** Trimolecular Fluorescence Complementation (TriFC) through co-expression of SR45:^{C}YFP or ACINUS:^{C}YFP with SAP18:^{N}YFP and a pMDC32 plasmid harboring no coding sequence (Ø, upper panels) or either the RRM of ACINUS (bottom left panel) or PININ (bottom right panel). Pictures represent the maximum intensity projections of 30 z-stack images from a 29.21 µm section (with a z-step size of 1.01 µm). The voltage of the EYFP PMT was set up at 700V in all experiments. For both BiFC **(A)** and TriFC **(B)** observations, representative images of fluorescence reveal the interaction of SR45 variants in the nucleus, nucleolus, and in speckles-like structures (arrowheads) in transient expression assay in tobacco leaf cells. At least three independent transient events were generated and analyzed, depicting similar fluorescence profiles. Scale bars = 10 µm. Red signals represent chlorophyll autofluoresence.

Figure 6. Subcellular localization of SR45-associated proteins. **(A)** Subcellular fluorescence distribution in transient expression assays in tobacco leaf cells upon N-terminal EGFP-tagging (except for SRPK4 which was C-terminally tagged). Scale bars = 10 µm. Red signals represent

chlorophyll autofluoresence. Whenever cytoplasmic and nuclear signals were detected, insets depict the detailed intranuclear localization. At least three independent transient events were generated and analyzed, depicting similar fluorescence profiles.

Figure 7. RNA motifs binding to the SR45 RRM. RNA motif 1 **(A)** and RNA motif 2 **(B)** identified through 4 rounds of SELEX selection with the RRM of SR45. Non-significant RNA motifs **(C)** identified using the mutated version of the RRM of SR45. The statistical significance (*E*-value) is indicated at the bottom of each consensus. Logos were redesigned using WebLogo (Crooks *et al.*, 2004). The fourth non-significant RNA motif (#4) identified using the mutated version of SR45 RRM (which presents the best *E*-value) is displayed here, but the three other RNA motifs (#1-3) are depicted in **Supplementary Figure S5**. All RNA motifs were discovered using the MEME tool (version 5.4.1).

Figure 8. A working model for the molecular function of SR45-binding proteins. Schematic diagram showing the different binding partners of SR45 identified in this study and the functional implications of these interactions. Green and red double-headed arrows indicate, respectively, the presence or the absence of interaction during directed Y2H experiments. Green circles represent positive trimeric complexes observed by Y3H experiments and TriFC *in planta*. The grey divider represents functional interconnection between nuclear complexes.

Supplementary Figure S1. Scaled schemes depicting the native *SR45* gene and mutant variants. RA1 and RA2 variants correspond to RS domains in which all the serines (39 in RS1 and 49 in RS2) were substituted in alanine, respectively as shown in **Supplementary Table S6**. Critical aromatic amino acids (bold underlined) connecting the RNA in RNP2 and RNP1 motifs were substituted in alanines (Califice *et al.*, 2012; Maris *et al.*, 2005; Stankovic *et al.*, 2016). 1-1245: *SR45* gene size in bp.

Supplementary Figure S2. Toxicity and autoactivation assays of the native SR45 and SR45 mutant variants on a –Trp/X-α-gal medium. Yeast transformants obtained using 100 ng of the following plasmids: **(A)** empty pGBTK7(+) vector, **(B)** pGBKT7:SR45.1, **(C)** pGBKT7:SR45.2, **(D)** pGBKT7(+):SR45mutRS1, **(E)** pGBKT7(+):SR45mutRRM, **(F)** pGBKT7(+):SR45mutRS2,

(G) pGBKT7(+):SR45mutRS1+RS2, **(H)** pGBKT7(+):SR45mutRS1+RRM, **(I)** pGBKT7(+):SR45mutRRM+RS2, and **(J)** pGBKT7(+):SR45mutRS1+RRM+RS2. Similar results were obtained for pGADT7(+) constructs.

Supplementary Figure S3. Reporter lines expressing *pSR45:EGFP*. The promoter is active in **(A-B)** hypocotyl **(A)** and cotyledons **(B)**, **(C)** two-week-old root vasculature and epidermis, **(D-F)** leaves, including epidermis and veins **(D)**, stomata [**(E)**, arrow] and trichome **(F)**, **(G-H)** gynoecium (valves, gynophore, abscission zone and receptacle) **(G)**, and stigma and style **(H)**, **(I)** androecium (anther and filament), **(J-K)** petals (epidermis and veins), and **(L)** sepal epidermis. Red signals represent chlorophyll autofluoresence. At least three independent T3 lines were generated and analyzed, depicting similar fluorescence profiles.

Supplementary Figure S4. SR45 interaction with Arabidopsis SR proteins. RSZ, SC35 and SR subfamilies (mammalian orthologs) comprise, respectively, from left to right: RSZ21, RSZ22, RSZ22a, SC35, SR30, SR34, SR34a and SR34b. RS2Z, SCL, RS and SR45 subfamilies (plant specific) comprise, respectively, from left to right: RS2Z32, RS2Z33, SCL28, SCL30, SCL30a, SCL33, RS31, RS31a, RS40, RS41, SR45.1 and SR45.2. From the mated culture, dilutions to an OD600 of 0.5 were spotted on -Trp/-Leu/-His/X-α-Gal/AurA agar plates. Positive interactions were confirmed by growth and blue staining.

Supplementary Figure S5. The mutated RRM of SR45 does not bind to a specific RNA consensus. Three of the four non-significant RNA motifs (#1-3) identified through 4 rounds of SELEX selection with the mutated version of SR45 RRM are displayed. The statistical significance (*E*-value) is indicated at the bottom of each consensus. Logos were redesigned using WebLogo (Crooks *et al.*, 2004). The fourth motif (#4) (which presents the best *E*-value) is depicted in **Figure 7**. All RNA motifs were discovered using the MEME tool (version 5.4.1) with 12 sequences.

Supplementary Figure S6. Trinucleotide frequency among the sequences used to identify SR45-associated RNA consensuses (related to **Figure 7**).

Supplementary Figure S7. RNA motifs binding to the RRMs of SR34. RNA motif consensuses identified through 4 rounds of SELEX selection with the RRMs of SR34 [RRM2 **(A)** or RRM1 **(B)**]. Non-significant RNA motifs identified using mutated versions of RRM2 **(C)** and RRM1 **(D)** of SR34. The statistical significance (*E*-value) is indicated at the bottom of each consensus. Logos were redesigned using WebLogo (Crooks *et al.*, 2004). All RNA motifs were discovered using the MEME tool (version 5.4.1). **(A)** The pseudo-RRM (RRM2) of SR34 recognized an invariant motif (5'-AGGGAG-3') succeeded by [G/A] and [A/G] nucleotides (*E*-value: 3.4×10^{-17}), and most of the sequences are containing the AGGGAGGA motif **(Supplementary Table S12)**. This motif is in complete agreement with previously uncovered RNA sequences specifically bound by the RRM2 of the human ortholog of SR34 (SRSF1) (Cléry *et al.*, 2013; Cléry *et al.*, 2021). **(B)** The canonical RRM (RRM1) of SR34 recognized an invariant sequence (5'-AUACA-3') flanked by and enriched in CN dinucleotides ('N' for any nucleotide) (*E*-value: 4.1×10^{-14}). This motif is again in agreement with a cytosine-rich motif preferentially bound by the RRM1 of SRSF1 (Cléry *et al.*, 2013; Cléry *et al.*, 2021). All sequences contained CA and CG dinucleotides **(Supplementary Table S13)**. A higher occurrence of CA dinucleotides preceding the invariant 5'-AUACA-3' was observed, predominantly in a single copy or sporadically in tandem. The CU dinucleotide was directly located after the invariant sequence in most of the cases and was usually present in a single copy. Similarly, the CG dinucleotide was mainly present in a single copy but was frequently spaced out by three nucleotides from the invariant CA dinucleotide. The least represented dinucleotide was CC.

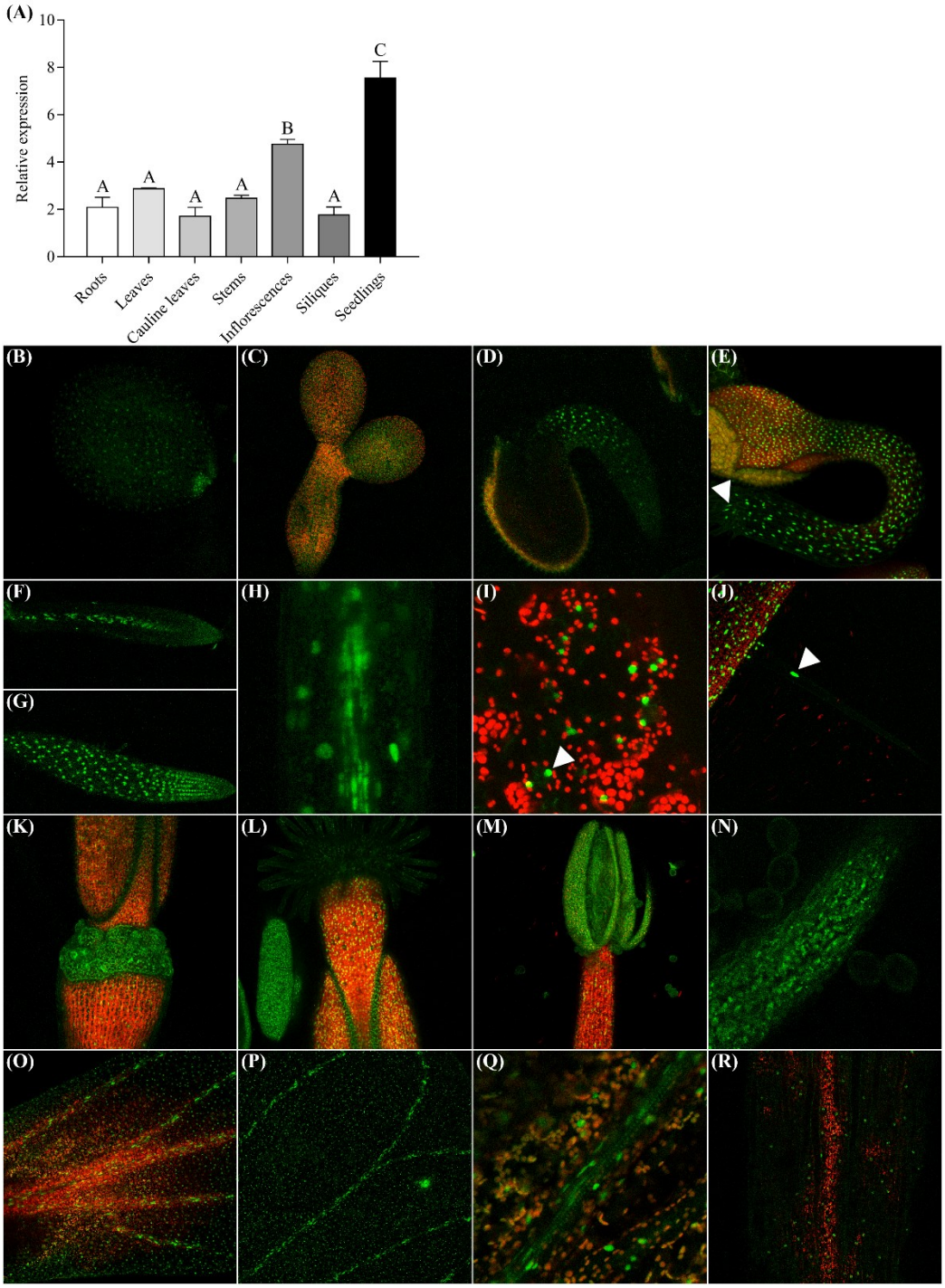

Figure 1. Expression profile of the *SR45* gene and of the corresponding protein. **(A)** Quantitative RT-PCR analyses of *SR45* gene expression in Arabidopsis vegetative and reproductive organs. Values represent means ± SEM (from three biological replicates, each consisting of pools of organs from three plants) and are relative to *AT1G58050*. Data were analyzed by one-way ANOVA followed by Dunnett multiple comparison post-tests. Statistically significant differences between means are indicated different letters ($P<0.05$). (**B-R**) Expression profile of the SR45 protein. The fusion protein SR45:GFP is expressed in **(B)** seed coat and hilum region, **(C)** embryo (cotyledons), **(D)** radicle, **(E)** young seedling (cotyledons and root, including root hairs as indicated by the arrow), **(F-H)** two-week-old root vasculature **(F, H)** and epidermis **(G)**, **(I-J)** leaves, including stomata [**(I)**, arrow] and trichome [**(J)**, arrow], **(K-L)** gynoecium (valves, gynophore, abscission zone and receptacle) **(K)**, and stigma and style **(L)**, **(M-N)** androecium (anther and filament), **(O-Q)** petals (epidermis and veins), and **(R)** sepal epidermis. Red signals represent chlorophyll autofluoresence. At least three independent T3 lines were generated and analyzed, depicting similar fluorescence profiles.

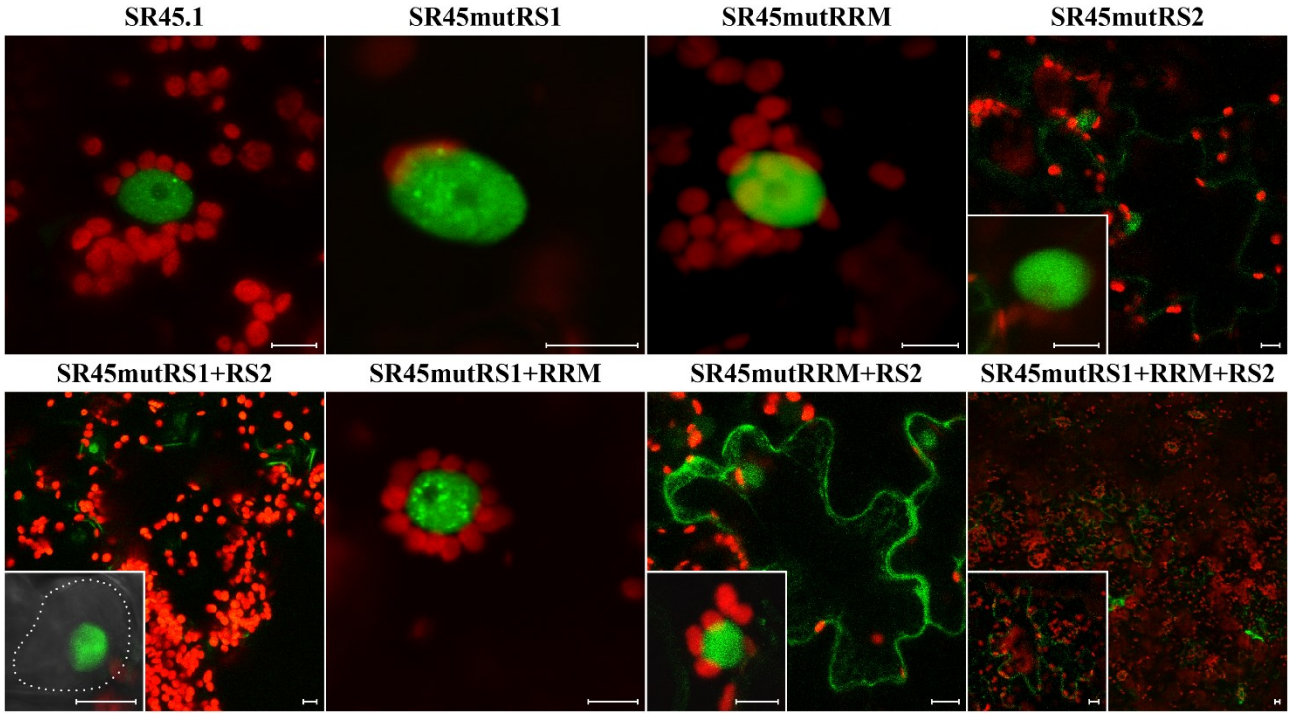

Figure 2. Structural determinants modulating SR45 localization. Subcellular fluorescence distribution in transient expression assays in tobacco leaf cells upon N-terminal EGFP-tagging of the native SR45 and SR45 mutant variants. Dotted lines delimit the nucleus. Scale bars = 10 µm. Red signals represent chlorophyll autofluoresence. Whenever cytoplasmic and nuclear signals were detected, insets depict the detailed intranuclear localization. At least three independent transient events were generated and analyzed, depicting similar fluorescence profiles.

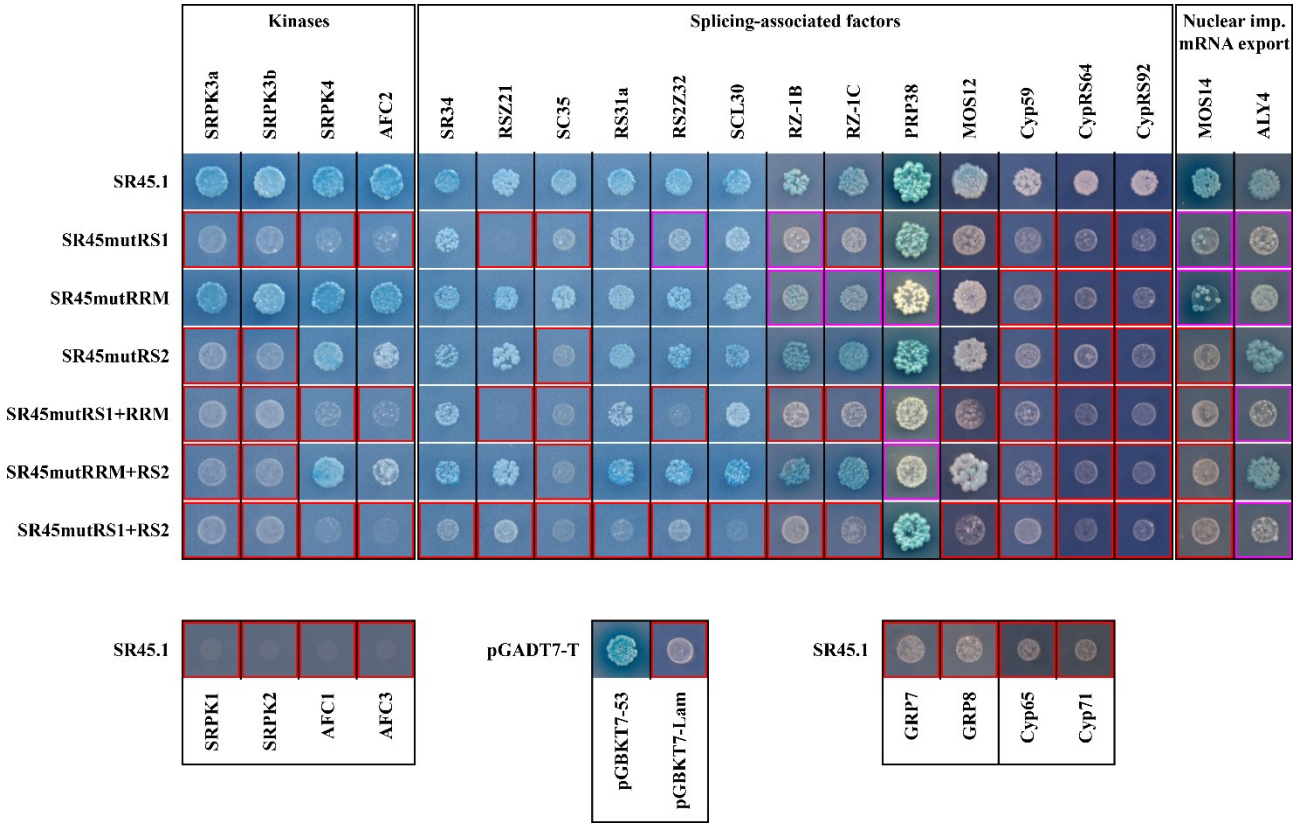

Figure 3. SR45 interactions detected by (directed) yeast two-hybrid screenings. From the mated culture, dilutions to an OD600 of 1 were spotted on -Trp/-Leu/-His/X-α-Gal/AurA agar plates. Positive interactions were confirmed by growth and blue staining as seen with the positive control (pGADT7-T x pGBKT7-53). Purple and red squares are indicative of a weakened or abolished interaction upon substitutions within the corresponding SR45 domain, respectively. A weakened interaction is characterized by the ability of several single colonies to grow, while an abolished interaction is characterized at most by a white halo of dead cells (similar to the negative control pGADT7-T x pGBKT7-Lam).

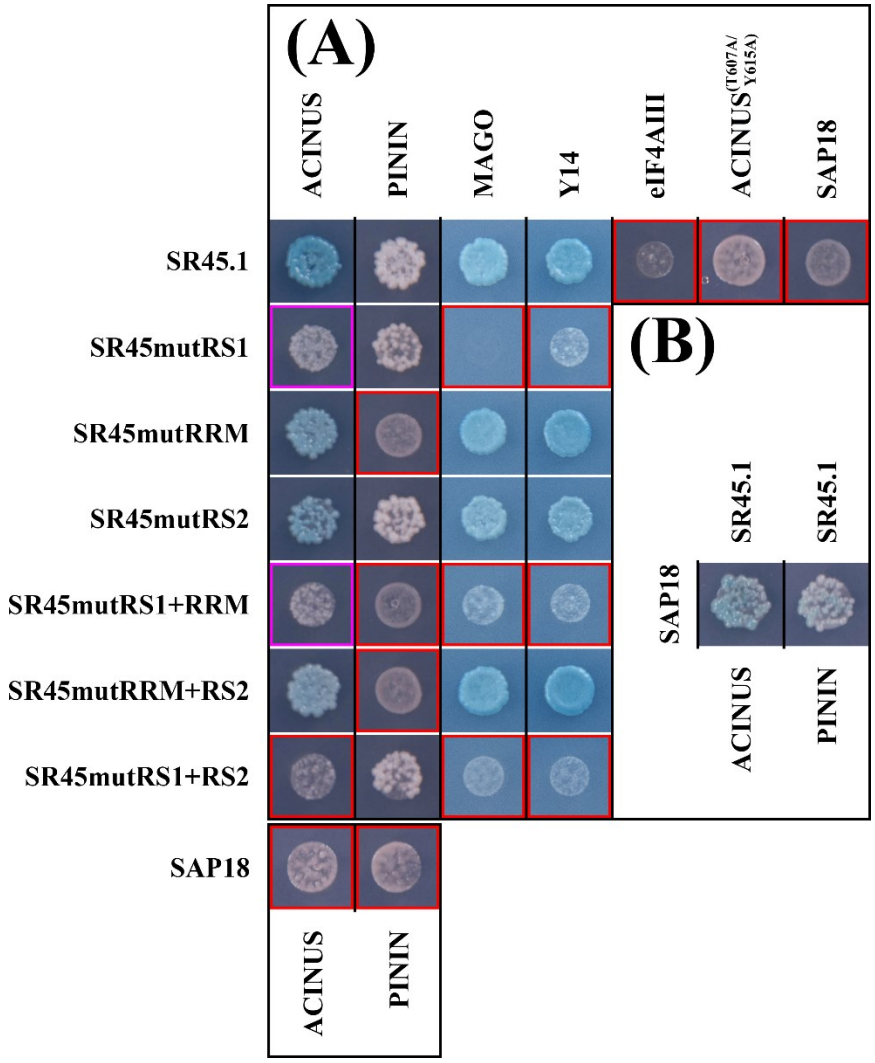

Figure 4. SR45 associates with EJC core components and peripheral factors. Interaction between the native SR45, and SR45 mutant variants, and ACINUS(RRM) and PININ (from plant ASAP and PSAP complexes, respectively), and EJC core components (MAGO and Y14) **(A)**. Ternary complexes formed in the simultaneous presence of SAP18, SR45 and either ACINUS(RRM) or PININ **(B)**. From the mated culture, dilutions to an OD600 of 1 were spotted on -Trp/-Leu/-His/X-α-Gal/AurA agar plates (for Y2H assays) **(A)** or -Met/-Trp/-Leu/-His /X-a-gal/Aureobasidin A (for Y3H assays) **(B)**. Positive interactions were confirmed by growth and blue staining. Purple and red squares are indicative of a weakened or abolished interaction upon substitutions within the corresponding SR45 domain, respectively. A weakened interaction is characterized by the ability of several single colonies to grow, while an abolished interaction is characterized at most by a white halo of dead cells.

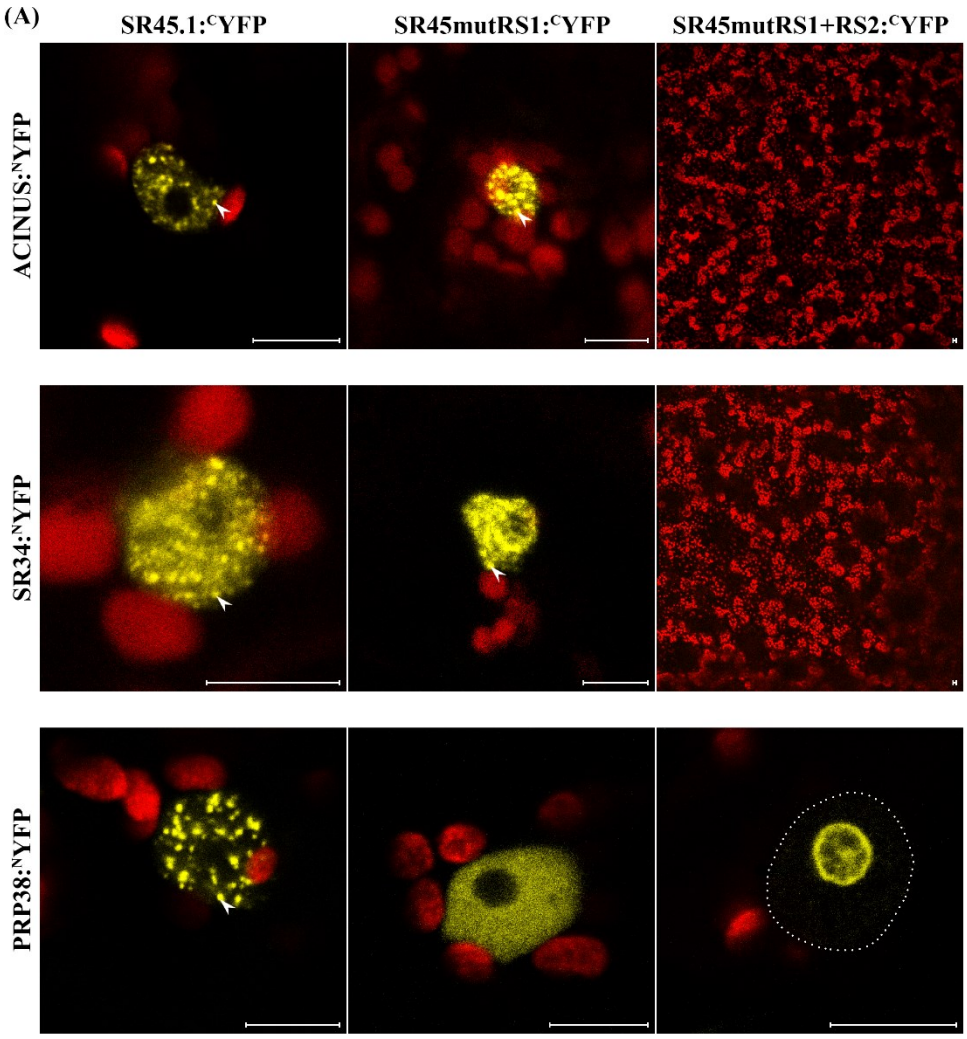

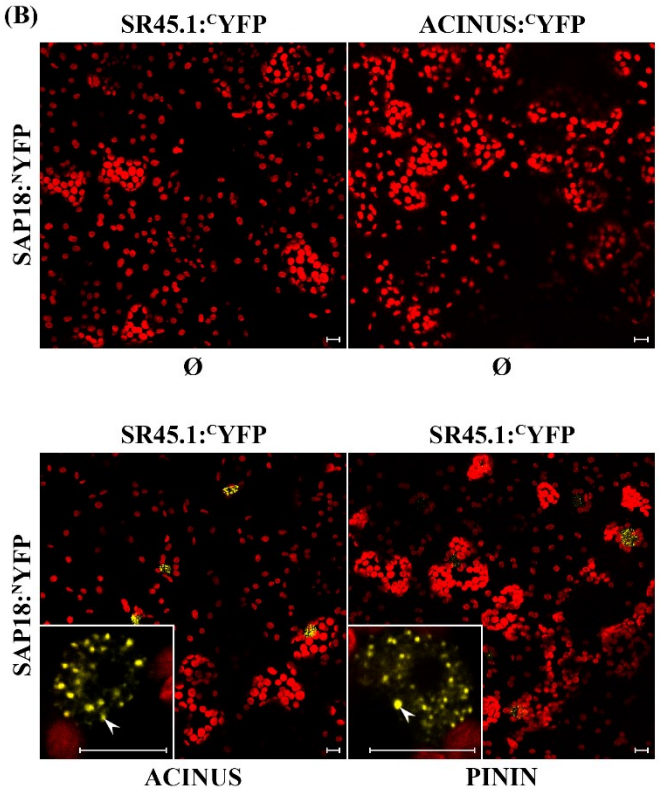

Figure 5. SR45 interacts with splicing factors and EJC peripheral factors in plant cells. **(A)** Bimolecular Fluorescence Complementation (BiFC) through co-expression of SR45 or SR45 mutant variants fused to the C-terminal half of YFP (SR45, SR45mutRS1, or SR45mutRS1+RS2:^{C}YFP) and ACINUS(RRM), SR34, or PRP38 fused to the N-terminal half of YFP (ACINUS(RRM), SR34, or PRP38:^{N}YFP). Dotted lines delimit the nucleus. **(B)** Trimolecular Fluorescence Complementation (TriFC) through co-expression of SR45:^{C}YFP or ACINUS:^{C}YFP with SAP18:^{N}YFP and a pMDC32 plasmid harboring no coding sequence (Ø, upper panels) or either the RRM of ACINUS (bottom left panel) or PININ (bottom right panel). Pictures represent the maximum intensity projections of 30 z-stack images from a 29.21 µm section (with a z-step size of 1.01 µm). The voltage of the EYFP PMT was set up at 700V in all experiments. For both BiFC **(A)** and TriFC **(B)** observations, representative images of fluorescence reveal the interaction of SR45 variants in the nucleus, nucleolus, and in speckles-like structures (arrowheads) in transient expression assay in tobacco leaf cells. At least three independent transient events were generated and analyzed, depicting similar fluorescence profiles. Scale bars = 10 µm. Red signals represent chlorophyll autofluoresence.

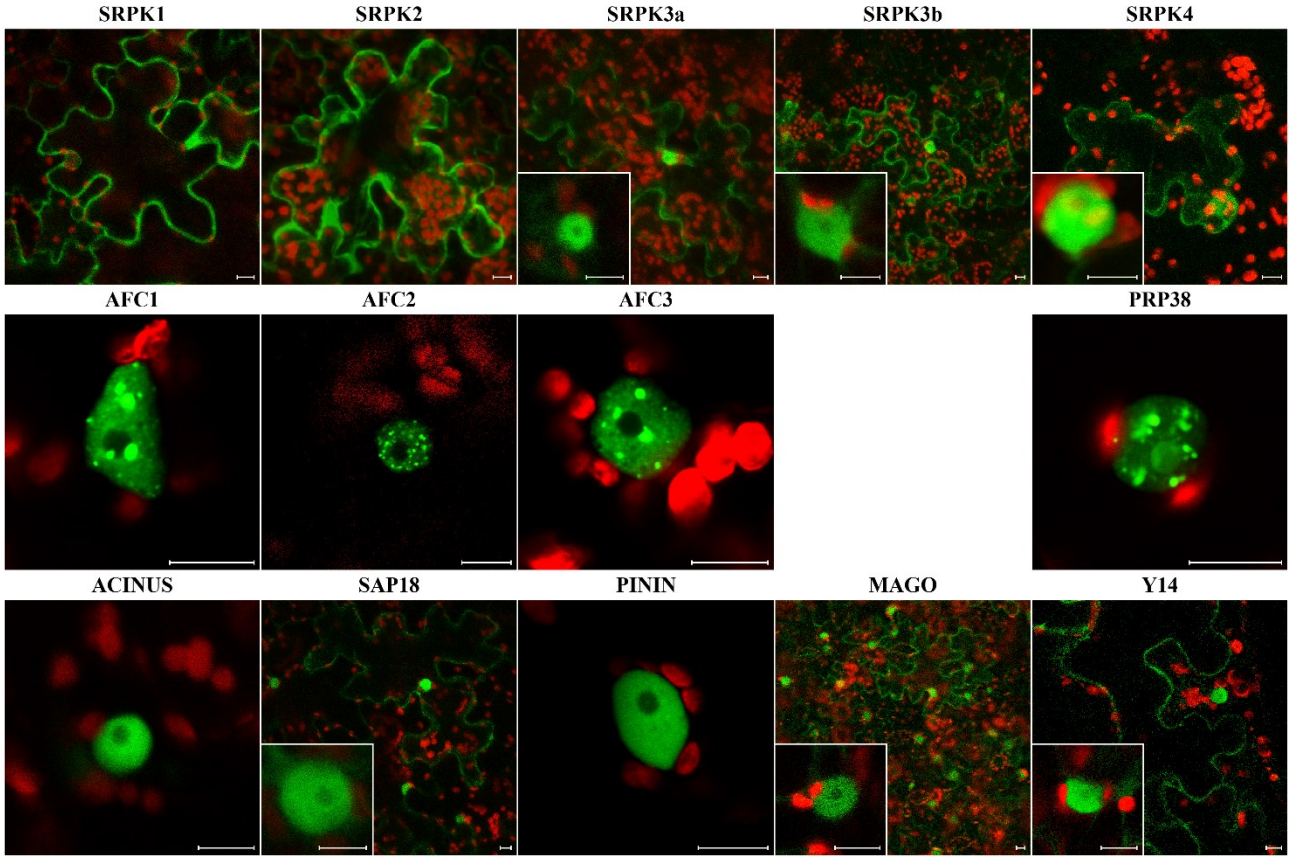

Figure 6. Subcellular localization of SR45-associated proteins. **(A)** Subcellular fluorescence distribution in transient expression assays in tobacco leaf cells upon N-terminal EGFP-tagging (except for SRPK4 which was C-terminally tagged). Scale bars = 10 µm. Red signals represent chlorophyll autofluoresence. Whenever cytoplasmic and nuclear signals were detected, insets depict the detailed intranuclear localization. At least three independent transient events were generated and analyzed, depicting similar fluorescence profiles.

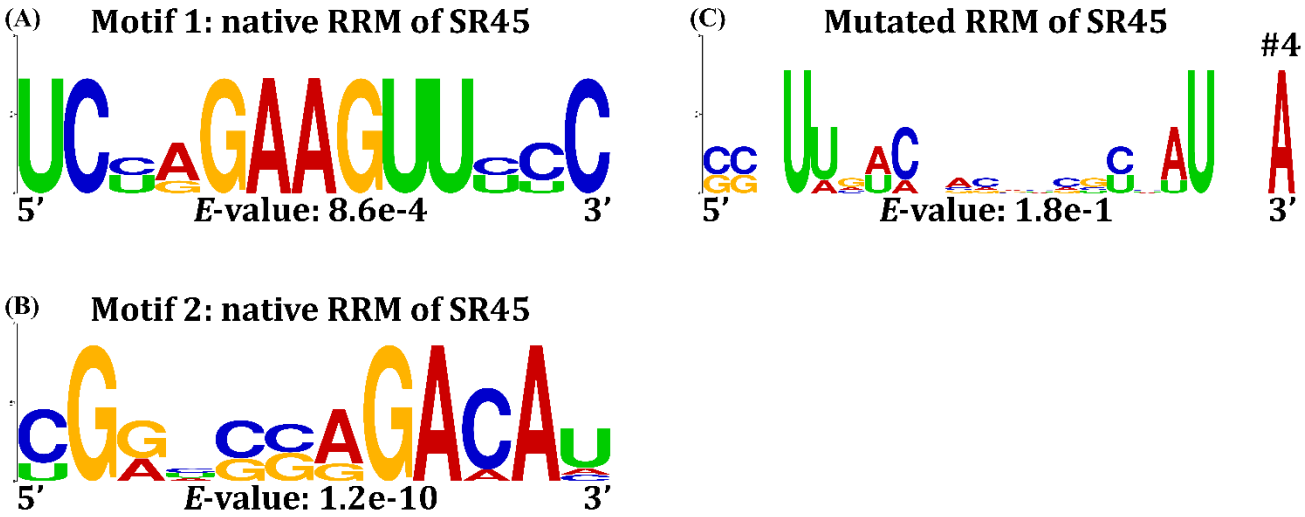

Figure 7. RNA motifs binding to the SR45 RRM. RNA motif 1 **(A)** and RNA motif 2 **(B)** identified through 4 rounds of SELEX selection with the RRM of SR45. Non-significant RNA motifs **(C)** identified using the mutated version of the RRM of SR45. The statistical significance (*E*-value) is indicated at the bottom of each consensus. Logos were redesigned using WebLogo (Crooks *et al.*, 2004). The fourth non-significant RNA motif (#4) identified using the mutated version of SR45 RRM (which presents the best *E*-value) is displayed here, but the three other RNA motifs (#1-3) are depicted in **Supplementary Figure S5**. All RNA motifs were discovered using the MEME tool (version 5.4.1).

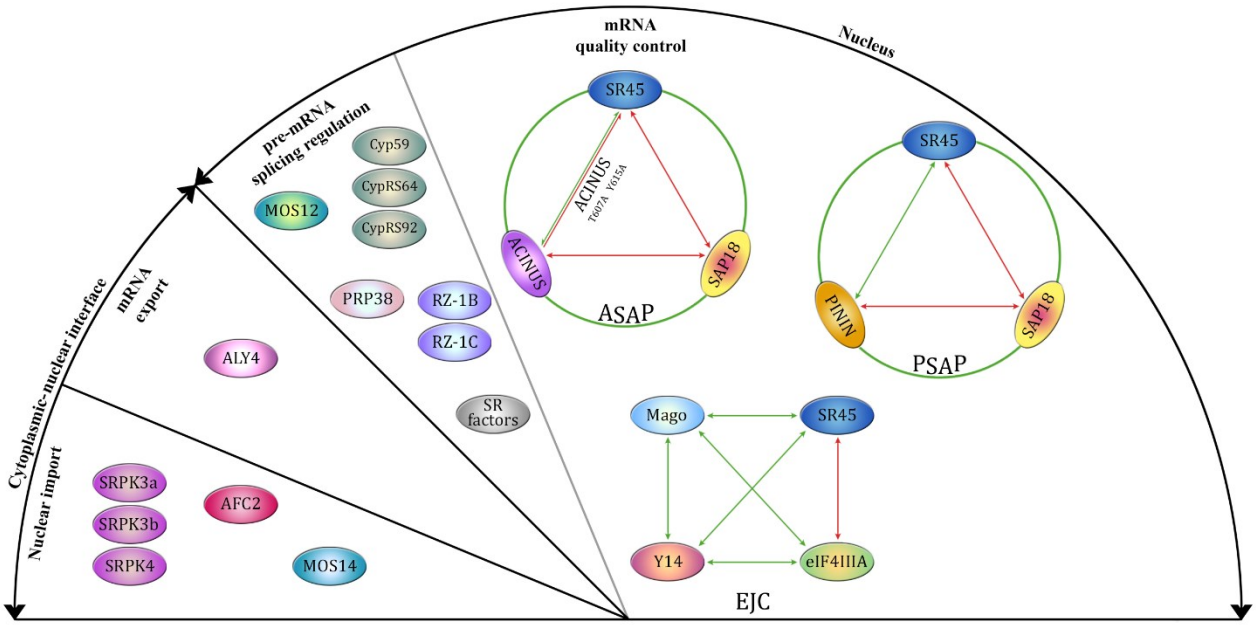

Figure 8. A working model for the molecular function of SR45-binding proteins. Schematic diagram showing the different binding partners of SR45 identified in this study and the functional implications of these interactions. Green and red double-headed arrows indicate, respectively, the presence or the absence of interaction during directed Y2H experiments. Green circles represent positive trimeric complexes observed by Y3H experiments and TriFC *in planta*. The grey divider represents functional interconnection between nuclear complexes.